NASA CONTRACTOR REPORT

NASA CR-27

NASA CR-2720

DEVELOPMENT OF AN OPTIMAL AUTOMATIC CONTROL LAW AND FILTER ALGORITHM FOR STEEP GLIDESLOPE CAPTURE AND GLIDESLOPE TRACKING

Nesim Halyo

Prepared by
UNIVERSITY OF VIRGINIA
Charlottesville, Va. 22901
for Langley Research Center

NATIONAL AERONAUTICS AND SPACE ADMINISTRATION • WASHINGTON, D. C. • AUGUST 1976

1. Report No.	2. Government Accession No.	3. Recipient's Catalog No.
NASA CR-2720		

4. Title and Subtitle	5. Report Date
Development of an Optimal Automatic Control Law and Filter Algorithm for Steep Glideslope Capture and Glideslope Tracking	August 1976
	6. Performing Organization Code
7. Author(s)	8. Performing Organization Report No.
Nesim Halyo	
	10. Work Unit No.
9. Performing Organization Name and Address	
University of Virginia Charlottesville, VA 22901	11. Contract or Grant No.
	NAS1-10210-6
	13. Type of Report and Period Covered
12. Sponsoring Agency Name and Address	Contractor Report
National Aeronautics & Space Administration Washington, DC 20546	14. Sponsoring Agency Code

15. Supplementary Notes

Final Report
Langley technical monitor: R. M. Hueschen

16. Abstract

A digital automatic control law to capture a steep glideslope and track the glideslope to a specified altitude is developed for the longitudinal/vertical dynamics of a CTOL aircraft using modern estimation and control techniques. The control law uses a constant gain Kalman filter to process guidance information from the Microwave Landing System (MLS), and acceleration from body mounted accelerometer data. The filter outputs navigation data and wind velocity estimates which are used in controlling the aircraft. Results from a digital simulation of the aircraft dynamics and the control law are presented for various wind conditions.

17. Key Words (Suggested by Author(s))	18. Distribution Statement
Optimal Control, 4D, Steep Approaches, Automatic Landing, Noise Abatement, Kalman Filtering, Approach	Unclassified - Unlimited Subject Category 02

19. Security Classif. (of this report)	20. Security Classif. (of this page)	21. No. of Pages	22. Price*
Unclassified	Unclassified	93	$4.75

*For sale by the National Technical Information Service, Springfield, Virginia 22161

Table of Contents

List of Figures

List of Tables

I. Introduction

This study considers the development of a digital 4D automatic control law to capture and follow a steep glideslope (6°) under low visibility conditions and in turbulence, using the Microwave Landing System (MLS) under development by the FAA. The study of curved 4D flight paths leading to a steep final approach under low visibility conditions is part of the Terminal Configured Vehicle program (TCV), sponsored jointly by NASA and FAA. The goals of the TCV program include the reduction of aircraft noise in airport communities, the reduction of fuel consumption, the reduction of the effects of adverse weather conditions on aircraft operations in air terminals, and the efficient use of airspace in congested terminal areas through the use of the Microwave Landing System.

The major effect of the use of steep glideslopes is in the area of noise reduction. In comparison to the currently used 2.5° to 3° ILS glideslopes, the 6° glideslope reduces the noise perceived on the ground due to its altitude profile and thrust level. At equal distances from the runway, the altitude of an aircraft following a 6° glideslope is almost twice the altitude of an aircraft following a 3° glideslope. Thus, the noise level heard on the ground is reduced due to the difference in altitude even when the same amount of noise is generated by both aircraft. A further reduction in noise is due to the fact that the aircraft flying the 6° glideslope generates less engine noise, so this steep glideslope requires a lower thrust setting than would be required by the same aircraft flying a 3° glideslope. This reduction in thrust level is of the order of 2:1 for the RSFS aircraft of the TCV program.

The reduction in thrust level associated with steep glideslopes also reduces the fuel consumed during the final approach. The ability to fly varying glideslope angles may also provide a method to avoid the vortex generated by large aircraft, by allowing smaller aircraft to fly different glideslopes to reduce the likelihood of such encounters; however, further research in this area is necessary. In general, the ability to fly steep glideslopes provides a versatility that can be useful in efficient use of airspace in the terminal area.

The guidance information necessary to fly steep glideslopes in low visibility instrument approaches can be obtained from the Microwave Landing System (MLS). The MLS is a ground-based guidance system which provides position information to aircraft inside its volumetric coverage. It consists of a DME providing range information, an azimuth antenna colocated with the DME providing the aircraft's azimuth angle relative to the runway up to $\pm 60^{\circ}$, and an elevation antenna located at the glide-path intercept point but offset to the side of the runway providing the aircraft's elevation angle up to 20°. A second elevation antenna located further down the runway to provide flare guidance is also under consideration. The MLS thus has a volumetric coverage, and provides guidance information that can be used for steep approaches and curved flight paths. The major characteristics of the MLS include high accuracy of position information, low sensitivity to adverse weather conditions and volumetric coverage.

With the high accuracy in position information provided by the MLS, it is of interest to investigate the use of low accuracy accelerometer

data in place of more sophisticated and costly systems such as inertial platforms in automatic landings under turbulent weather conditions. Thus, in this study, body-mounted accelerometers were used to provide acceleration information. This information was mixed with MLS data arriving at discrete instants of time and with air data in a constant gain Kalman filter to obtain optimal estimates of the aircraft velocity and sink rate as well as the wind velocities by filtering out the noise associated with the various sensors. The development of this filter for the longitudinal axis is given in Section III.B. The results obtained from a simulation of the filter are shown in Section V.

In Section II, the aircraft's equations of motion used in the simulation are described. A mathematical model describing the deviations of the aircraft's longitudinal variables from their steady values on a 6° glideslope is obtained. The effect of lags in thrust build-up and the effects of winds on the aircraft motion are included in this model. Using the Dryden spectrum, a dynamical model for the simulation of wind gusts is developed, then steady winds are added to this model. The models are expressed in state variable form which is more suitable to the use of modern estimation and control techniques.

In Section III, a mathematical model for the noises in the various sensors is developed. Then a non-linear pre-processor is used to transform these measurements into a form more suitable for filtering purposes. In Section III.B, the development of the filter is described and some aspects of its implementation are discussed.

In Section IV, a digital automatic control law to capture and follow a 6° glideslope is developed for the longitudinal axis. The control law uses the aircraft variables as well as the wind estimates to decrease the aircraft's deviations from the glidepath.

Section V describes the results obtained from a simulation of the aircraft, winds, sensor errors, the filter and the control law.

It is a pleasure to acknowledge Dr. Thomas M. Walsh for his encouragement of the concepts presented in this study.

II. Modelling of Aircraft Dynamics and Winds

The general equations of motion for aircraft are complex nonlinear differential equations and can be found in various texts on aircraft dynamics [4], [5], [6]. As this study considers the glideslope capture and glideslope phases of the final approach, however, several simplifying assumptions can be made to reduce the complexity of these equations and make them more amenable to analytic manipulations without appreciable degradation in their validity [4, p. 230], [5, pp. 254-265]. As the equations of motion are used extensively in the study and the computer simulation, the specific equations used will be described here.

A. Aircraft dynamics with wind disturbances

The phase of flight considered in this study is glideslope capture followed by a steep glideslope up to 6 degrees flown at a constant airspeed of 120 knots except for small fluctuations. In these phases of flight (Fig. 1) the aircraft is aligned with the runway, has a zero or very small yaw angle with respect to the runway as well as a zero bank angle except for the case of a significant cross-wind requiring a "crab" maneuver. The control activity for the lateral motion is aimed at keeping the aircraft aligned with the runway, with level wings. Hence, all the lateral variables, i.e. yaw, roll, their rates and the sideslip angle, have very small values except for crab maneuvers. Similarly, among the longitudinal variables, the pitch angle is small during these phases of flight, usually within 6° to -4° for a 6° capture.

Under these conditions, the nonlinear equations of motion can be linearized about the steady state flight condition of the glideslope using well-known methods [4], [5], [6]. The deviations from the steady

flight condition can be described by linear differential equations which are simpler to use in analytical manipulations and are more suitable for the application of modern control theory principles. Under the conditions stated above (these conditions will be restated more precisely below), the equations of motion of the aircraft can be expressed as [2, p. 2.32]:

$$m(\dot{u} - V_o r - R_o v + W_o q + Q_o \omega) = -mg \cos\theta_o \theta + f_{A_x} + f_{T_x}, \tag{1}$$

$$m(\dot{v} + U_o r + R_o u - W_o p - P_o \omega) = -mg \sin\Phi_o \sin\theta_o \theta + mg \cos\Phi_o \cos\theta_o \phi + f_{A_y} + f_{T_y}, \tag{2}$$

$$m(\dot{\omega} - U_o q - Q_o u + V_o p + P_o v) = -mg \cos\Phi_o \sin\theta_o \theta - mg \sin\Phi_o \cos\theta_o \phi + f_{A_z} + f_{T_z}, \tag{3}$$

$$I_{xx}\dot{p} - I_{xz}\dot{r} - I_{xz}(P_o q + Q_o p) + (I_{zz} - I_{yy})(R_o q + Q_o r) = \ell_A + \ell_T, \tag{4}$$

$$I_{yy}\dot{q} + (I_{xx} - I_{zz})(P_o r + R_o p) + 2I_{xz}(P_o p - R_o r) = m_A + m_T, \tag{5}$$

$$I_{zz}\dot{r} - I_{xz}\dot{p} + (I_{yy} - I_{xx})(P_o q + Q_o p) + I_{xz}(Q_o r + R_o q) = n_A + n_T, \tag{6}$$

where

U_o = steady state inertial speed in the x direction

V_o = steady state inertial speed in the y direction

W_o = steady state inertial speed in the z direction

u = perturbation in the inertial speed in the x direction

v = perturbation in the inertial speed in the y direction

w = perturbation in the inertial speed in the z direction

P_o = steady state roll rate

Q_o = steady state pitch rate

R_o = steady state yaw rate

p = perturbation in roll rate

q = perturbation in pitch rate

r = perturbation in yaw rate

Φ_o = steady state roll angle

Θ_o = steady state pitch angle

Ψ_o = steady state yaw angle

ϕ = perturbation in roll angle

θ = perturbation in pitch angle

ψ = perturbation in yaw angle

f_{A_x} = perturbation in net aerodynamic force along the x direction

f_{A_y} = perturbation in net aerodynamic force along the y direction

f_{A_z} = perturbation in net aerodynamic force along the z direction

f_{T_x} = perturbation in thrust along the x direction

f_{T_y} = perturbation in thrust along the y direction

f_{T_z} = perturbation in thrust along the x direction

ℓ_A = perturbation in rolling moment due to aerodynamic forces

m_A = perturbation in pitching moment due to aerodynamic forces

n_A = perturbation in yawing moment due to aerodynamic forces

ℓ_T = perturbation in rolling moment due to thrust

m_T = perturbation in pitching moment due to thrust

n_T = perturbation in yawing moment due to thrust

These equations are valid for any set of right-handed rectangular body-fixed axes, i.e., right-handed reference frame fixed to the body of the aircraft with the origin located at the aircraft's center of mass. Figure 2 shows the sign conventions and the vectors pictorially for the vertical plane. The assumptions and approximations used in arriving at equations (1) - (6) are given below.

1. The earth is assumed to be flat and fixed in an inertial reference frame;

2. The perturbations in the angles are small, so that

$$\cos\theta \simeq \cos\phi \simeq 1 \tag{7}$$

$$\sin\theta \simeq \theta, \ \sin\phi \simeq \phi; \tag{8}$$

3. The second order terms in the perturbations are negligible relative to the first order terms in the perturbations;

4. The aircraft is a rigid body.

In this form, equations (1) - (6) are coupled; however, if the steady state flight condition is taken to be the glideslope, these

equations can be decoupled and simplified. This steady state flight is described by:

$$\Phi_o = P_o = Q_o = R_o = V_o = 0 \tag{9}$$

Hence, for this steady flight condition, the equations of motion simplify to:

$$m(\dot{u} + W_o q) = -mg \cos\Phi_o \theta + f_{A_x} + f_{T_x} \tag{10}$$

$$m(\dot{\omega} - U_o q) = -mg \sin\Phi_o \theta + f_{A_z} + f_{T_z} \tag{11}$$

$$I_{yy}\dot{q} = m_A + m_T \tag{12}$$

$$m(\dot{v} + U_o r - W_o p) = mg \cos\Phi_o \phi + f_{A_y} + f_{T_y} \tag{13}$$

$$I_{xx}\dot{p} - I_{xz}\dot{r} = \ell_A + \ell_T \tag{14}$$

$$I_{zz}\dot{r} - I_{xz}\dot{p} = n_A + n_T \tag{15}$$

Equations (10) - (12) contain only longitudinal variables, whereas Eqns. (13) - (15) contain only lateral variables so that the equations are now decoupled. As this study is concerned with glideslope capture and glideslope tracking, only the longitudinal equations of motion (i.e., Eqns. (10) - (12)) will be considered in the following.

Throughout this study, mainly three sets of coordinate axes will be used: the earth fixed axis, the body axis and the stability axes. The earth-fixed coordinate frame (x_e, y_e, z_e) has its origin fixed on a specified point on the runway at which the aircraft is going to land; the x_e axis is along the runway, the direction in which the aircraft will land being positive; i.e., at touchdown the A/C will have a positive veolcity along x_e. The z_e axis is vertical positive downwards; and y_e is perpendicular to both x_e and z_e with the positive end in the direction to make the coordinate frame right-handed. As the earth is assumed to be stationary with respect to an inertial frame, (x_e, y_e, z_e) is itself an inertial frame.

Two body-fixed axes with their origin fixed at the center of mass of the A/C are also used: the body (x_b, y_b, z_b) and stability (x_s, y_s, z_s) axes. The x_b axis is in the A/C's plane of symmetry and is taken to be along the fuselage reference line of the A/C, positive towards the nose; the y_b axis is positive towards the right wing, and z_b is positive downwards; this reference frame will be referred to as the body axes. The stability axes (x_s, y_s, z_s) can be obtained from the body axes by a rotation of α_o about the y_b axis such that when the A/C is in its steady state flight condition, its velocity vector is along the positive x_s axis. The equations of motion for the aircraft (10 - 12) will be written in the stability axes.

In the above equations, the term f_{A_x} represents the total algebraic change in the value of the aerodynamic force along the x_s axis due to changes in the values of the aerodynamic and control surface variables;

the changes in the forces and variables are referenced to the steady state values of the corresponding forces and variables. The remaining terms in equations (10 - 12) are defined similarly. For the longitudinal eqns. of motion, the aerodynamic forces and moments involved are the lift and drag forces and the pitching moment; the effects of thrust are described separately by the terms with subscript T. These forces and moments can be expressed as follows:

$$L = C_L(\underline{u}, \underline{\alpha}, \dot{\underline{\alpha}}, \underline{q}, \delta e, \delta s)\bar{q}S \tag{16}$$

$$D = C_D(\underline{u}, \underline{\alpha}, \dot{\underline{\alpha}}, \underline{q}, \delta e, \delta s)\bar{q}S \tag{17}$$

$$T = C_T(\underline{u}, \underline{\alpha}, \dot{\underline{\alpha}}, \underline{q})\bar{q}S \tag{18}$$

$$M = C_M(\underline{u}, \underline{\alpha}, \dot{\underline{\alpha}}, \underline{q}, \delta e, \delta s, \delta T)\bar{q}S\bar{c} \tag{19}$$

$$\bar{q} = \frac{1}{2}\rho V_a^2$$

where L, D, T and M represent the lift, drag, thrust forces and the pitching moment respectively, $\bar{q}$ is the dynamic pressure, V_a the airspeed, $\underline{u}$ the perturbation of V_a's component along the x_s axis, $\underline{\alpha}$ the perturbation in the angle of attack, $\dot{\underline{\alpha}}$ the time rate of change of $\underline{\alpha}$, $\underline{q}$ the pitch rate of the A/C relative to the atmosphere, δe the perturbation in the elevator surface deflection, δ_s the perturbation in the stabilizer surface deflection, δT the perturbation in the thrust force, S the wing area and

$\bar{c}$ the mean aerodynamic chord. Note that the aerodynamic forces and moments depend on the motion of the aircraft relative to the atmosphere such as $\underline{u}$, $\underline{\alpha}$, etc., rather than the inertial motion variables u, ω, etc. Thus the effect of winds is automatically included into the equations of motion. If the perturbation in the angle of attack of the inertial velocity, say α, is defined as

$$\alpha \triangleq \tan^{-1}\frac{\omega}{U_o + u} \cong \frac{\omega}{U_o}, \quad \omega << U_o, \; u << U_o, \tag{21}$$

then

$$\underline{u} = u + u_w, \; \underline{u}' = \frac{\underline{u}}{U_o} = u' + u_w' \tag{22}$$

$$\underline{\alpha} = \alpha + \alpha_w, \tag{23}$$

$$\dot{\underline{\alpha}} = \dot{\alpha} + \dot{\alpha}_w, \tag{24}$$

$$\underline{q} = q + q_w, \tag{25}$$

where the subscript w denotes the component due to winds.

Using Figure 2, it is seen that the total aerodynamic forces along the x_s and z_s axes are

$$F_{Ax_s} = L\sin\underline{\alpha} - D\cos\underline{\alpha} \tag{26}$$

$$F_{Az_s} = -L\cos\underline{\alpha} + D\sin\underline{\alpha} \tag{27}$$

The forces due to thrust are

$$F_{Tx_s} = T\cos(\alpha_o + \phi_T) \tag{28}$$

$$F_{Tz_s} = -T\sin(\alpha_o + \phi_T). \tag{29}$$

From these equations, we can obtain expressions for the perturbed force and moments by using a Taylor series where second and higher order terms are neglected, hence,

$$f_{Ax_s} \cong \frac{\partial F_{Ax_s}}{\partial \underline{u}}\underline{u} + \frac{\partial F_{Ax_s}}{\partial \underline{\alpha}}\underline{\alpha} + \frac{\partial F_{Ax_s}}{\partial \dot{\underline{\alpha}}}\dot{\underline{\alpha}} + \frac{\partial F_{Ax_s}}{\partial \underline{q}}\underline{q} + \frac{\partial F_{Ax_s}}{\partial \delta e}\delta e + \frac{\partial F_{Ax_s}}{\partial \delta s}\delta s \tag{30}$$

where the partial derivatives are evaluated at the steady state condition. Similarly, f_{Az_s}, f_{Tx_s}, f_{Tz_s}, m_A and m_T can be expressed by a truncated Taylor series of the same form. The partial derivatives in these expressions can be expressed in terms of the partial derivatives of the lift, drag, thrust and pitching moment coefficients, i.e., the stability derivatives. The equations of motion thus obtained are given below.

$$\begin{aligned} m\dot{u} = -mg\cos\theta_o\theta + \bar{q}_o S\{&(-C_{D\underline{u}'} + 2C_{Do} + C_{Tx\underline{u}'} + 2C_{Txo})\underline{u}' \\ &+ (C_{Lo} - C_{D\underline{\alpha}})\underline{\alpha} - C_{D\delta e}\delta e - C_{D\delta s}\delta s + C_{Tx\delta T}\delta T\} \end{aligned} \tag{31}$$

$$m(\dot{\omega} - U_o q) = -mg \sin\theta_o \theta + \bar{q}_o S\{-(C_{L_{\underline{u}}} + 2C_{L_o})\underline{u}' - (C_{L_\alpha} + C_{D_o})\underline{\alpha}$$

$$- C_{L_{\dot{\alpha}}}\underline{\dot{\alpha}} - C_{L_q}\underline{q}\}\{-C_{L_{\delta e}}\delta e - C_{L_{\delta s}}\delta s + C_{T_{z_{\delta T}}}\delta T\} \tag{32}$$

$$I_{yy}\dot{q} = \bar{q}_o S\bar{c}\{(C_{M_{\underline{u}}} + 2C_{M_o})\underline{u}' + (C_{M_{\underline{\alpha}}} + C_{MT_{\underline{\alpha}}})\underline{\alpha} + C_{M_{\dot{\alpha}}}\underline{\dot{\alpha}}$$

$$+ C_{M_q}\underline{q} + C_{M_{\delta e}}\delta e + C_{M_{\delta s}}\delta s + C_{M_{\delta T}}\delta T\}, \tag{33}$$

where W_o has been taken to be zero. After some manipulation, these equations can be expressed in state variable form. However, we shall first derive some further equations and include those as well in the state variable model.

First note that the flight path angle, γ, shown in Figure 2 can be expressed as

$$\gamma = \theta_o + \theta - (\alpha_o + \alpha) = (\theta_o - \alpha_o) + (\theta - \alpha) = \gamma_o + (\theta - \alpha) \tag{34}$$

Now, let (x,z) be the coordinates of the aircraft's center of mass along the earth-fixed coordinate frame x_e and z_e. Then the ground speed, $\dot{x}$, and the sink rate, $\dot{z}$, are given by

$$\dot{x} = V_i \cos\gamma = V_i \cos(\gamma_o + \theta - \alpha) \tag{35}$$

$$= V_i \cos\alpha \cos(\gamma_o + \theta) + V_i \sin\alpha \sin(\gamma_o + \theta) = U\cos(\gamma_o + \theta) + W\sin(\gamma_o + \theta) \tag{36}$$

$$\dot{z} = -V_i \sin\gamma = -U\sin(\gamma_o + \theta) + W\cos(\gamma_o + \theta) \tag{37}$$

Since the stability axis is chosen to correspond to the glideslope, the ground speed, x_o, and the sink rate, z_o, of the aircraft in the steady state condition are given by

$$\dot{x}_o = U_o \cos\gamma_o, \tag{38}$$

$$\dot{z}_o = -U_o \sin\gamma_o, \tag{39}$$

as in this steady state condition the speed along the z_s axis (i.e., W_o) is zero. Hence, the perturbation in the ground speed and sink rate are

$$\dot{x} - \dot{x}_o = (\dot{x} - \dot{x}_o) = U\cos(\gamma_o + \theta) + W\sin(\gamma_o + \theta) - U_o\cos\gamma_o \tag{40}$$

$$\dot{z} - \dot{z}_o = (\dot{z} - \dot{z}_o) = -U\sin(\gamma_o + \theta) + W\cos(\gamma_o + \theta) + U_o\sin\gamma_o \tag{41}$$

Substituting the equations

$$U = U_o + u, \quad W = W_o + \omega = \omega, \tag{42}$$

into (40) and (41),

$$\frac{(\dot{x} - \dot{x}_o)}{U_o} = [\cos(\gamma_o + \theta) - \cos\gamma_o] + u'\cos(\gamma_o + \theta) + \frac{\omega}{U_o}\sin(\gamma_o + \theta) \tag{43}$$

$$\tilde{=} - \sin\gamma_o\theta + \cos\gamma_o u' + \sin\gamma_o\alpha; \tag{44}$$

$$\frac{(\dot{z} - \dot{z}_o)}{U_o} = -[\sin(\gamma_o + \theta) - \sin\gamma_o] - u'\sin(\gamma_o + \theta) + \frac{\omega}{U_o}\cos(\gamma_o + \theta) \tag{45}$$

$$\cong -\cos\gamma_o\theta - \sin\gamma_o u' + \cos\gamma_o\alpha. \tag{46}$$

Thus the perturbations in ground speed and sink rate can be expressed as linear functions of θ, u' and α by (44) and (46) as long as the perturbations in the pitch angle, θ, are small. Note that the perturbations $(x(t) - x_o(t))$ and $(z(t) - z_o(t))$ in ground distance and altitude correspond to the variable time, i.e. $x(t) - x_o(t)$, is the perturbation or error in the x position of the aircraft relative to where it should have been at that time. Hence, if these errors are zero, the aircraft not only keeps an average inertial speed of U_o, but also has to be at specified positions at the appropriate time; i.e. $x - x_o$, $z - z_o$ represent 4D (four dimensional) errors which include time as a variable.

To include the effects of the servo responses of the actuators, we shall also model the thrust and stabilizer motions dynamically by linear equations. Thus,

$$\dot{\delta T} = -.5\delta T + .298\delta th \tag{47}$$

$$\delta th = u_3 \ , \quad \dot{\delta s} = u_2 \tag{48}$$

where δT, δth and δs are perturbations of thrust, throttle and stabilizer from their steady state value, respectively. The elevator

is not modeled in this fashion as its motion is relatively fast, i.e. its time constant is much lower than the others. Thus the thrust model takes the "spool up" time of the engine into account, at least linearly.

Now, the equations of motion of the aircraft, the 4D perturbations in the ground speed and sink rate and the effects of the actuator responses can be combined into a state variable model. Let the state vector x be defined as

$$x' = (\theta \quad u' \quad \alpha \quad q \quad \frac{x - x_o}{U_o} \quad \frac{z - z_o}{U_o} \quad \delta T \quad \delta th \quad \delta s) \tag{49}$$

Then equations (31) - (33), (44), (46) - (48) can be combined into the vector equation

$$\dot{x} = Ax + Bu + Dw \tag{50}$$

where $u' = (\delta e \quad \delta\dot{s} \quad \delta\dot{th})$, $w = (u_w' \quad \alpha_w \quad q_w)$ and A , B and D correspond to the appropriate coefficients in the original equations and are given below

$$A = \begin{bmatrix} 0 & 0 & 0 & 1 & 0 & 0 & 0 & 0 & 0 \\ a_{21} & a_{22} & a_{23} & 0 & 0 & 0 & a_{27} & 0 & a_{29} \\ a_{31} & a_{32} & a_{33} & a_{34} & 0 & 0 & a_{37} & 0 & a_{39} \\ a_{41} & a_{42} & a_{43} & a_{44} & 0 & 0 & a_{47} & 0 & a_{49} \\ -\sin\gamma_o & \cos\gamma_o & \sin\gamma_o & 0 & 0 & 0 & 0 & 0 & 0 \\ -\cos\gamma_o & -\sin\gamma_o & \cos\gamma_o & 0 & 0 & 0 & 0 & 0 & 0 \\ 0 & 0 & 0 & 0 & 0 & 0 & a_{77} & a_{78} & 0 \\ 0 & 0 & 0 & 0 & 0 & 0 & 0 & 0 & 0 \\ 0 & 0 & 0 & 0 & 0 & 0 & 0 & 0 & 0 \end{bmatrix}$$

$$B = \begin{bmatrix} 0 & 0 & 0 \\ b_{21} & 0 & 0 \\ b_{31} & 0 & 0 \\ b_{41} & 0 & 0 \\ 0 & 0 & 0 \\ 0 & 0 & 0 \\ 0 & 0 & 0 \\ 0 & 0 & 1 \\ 0 & 1 & 0 \end{bmatrix}, \quad D = \begin{bmatrix} 0 & 0 & 0 \\ a_{22} & a_{23} & 0 \\ a_{32} & a_{33} & d_{33} \\ a_{42} & a_{43} & d_{43} \\ 0 & 0 & 0 \\ 0 & 0 & 0 \\ 0 & 0 & 0 \\ 0 & 0 & 0 \\ 0 & 0 & 0 \end{bmatrix}$$

The expressions for the elements of the matrices A, B and D are given in the Appendix. Hence, the aircraft equations of motion along with 4D error equations in ground speed and sink rate have been modeled by a linear state variable model. It sould be noted, however, that the equations have been obtained by linearization of the nonlinear equations about the steady flight condition of a glideslope with angle γ_o and a constant airspeed U_o; hence, these equations provide a realistic model of the aircraft motion provided that the deviations from this steady flight condition are small.

B. Wind Modeling

To complete the aircraft model given by (50), the wind vector w has to be specified. The components of this vector consist of u_w', the normalized wind velocity in the $-x_s$ direction; α_w. the part of the angle of attack due to winds, and q_w, the rotation of the atmosphere about the y_s axis. The u_w' and α_w components are modeled as consisting of a gust component with zero average value and a steady component (i.e. the average value u_w' and α_w). Hence,

$$u'_w = u'_g + u'_s = (u_g + u_s)/V_a \tag{51}$$

$$\alpha_w = \alpha_g + \alpha_s = -(\omega_g + \omega_s)/V_a \tag{52}$$

where V_a is the airspeed.

The gust components can be modeled using the well-known Dryden spectrum [4]. This method consists of using spectral factorization methods to obtain a dynamical system which generates a random process having the specified power spectral density when driven by white noise. Let $u_g(t)$ be the gust velocity with respect to earth at time t; then the covariance function of the random process $u_g(t)$ is defined as

$$R_{u_g}(\tau) = E(u_g(t)u_g(t + \tau)), \tag{53}$$

where $u_g(t)$ is assumed to be a wide-sense stationary random process with zero mean and E denotes the statistical expectation operator [7], [8]. The power spectral density of this process is then defined as the Fourier transform of its covariance function $R_{u_g}(\tau)$:*

$$S_{u_g}(\omega) = \int_{-\infty}^{\infty} R_{u_g}(t)e^{-j\omega t}dt; \; j = \sqrt{-1}; \tag{54}$$

then, the variance of $u_g(t)$ or the power of the random process is given by

* Definitions of the Fourier transform differing from (54) by the factors $1/2\pi$, $1/\sqrt{2\pi}$, $2/\pi$ are sometimes used in the literature, we shall use the definition given above.

$$R_{u_g}(0) = \frac{1}{2\pi}\int_{-\infty}^{\infty} S_{u_g}(\omega)d\omega. \tag{55}$$

The Dryden spectra describe the statistical behavior of the wind gust velocities in the aircraft body coordinates by specifying their power spectral densities in terms of the spatial frequency Ω, [9].

$$S_u(\Omega) = \frac{2\sigma_u^2 L_u}{1 + (L_u\Omega)^2}, \tag{56}$$

$$S_\alpha(\Omega) = \frac{\sigma_\omega^2 L_\omega}{V_a^2} \frac{1 + 3(L_\omega\Omega)^2}{[1 + (L_\omega\Omega)^2]^2}, \tag{57}$$

$$S_q(\Omega) = \frac{\Omega^2 V_a^2}{1 + (\frac{4b}{\pi}\Omega)^2} S_{\alpha_g}(\Omega), \tag{58}$$

where b is the wing span, L_u and L_ω are the scales of turbulence, and Ω is the spatial frequency related to the temporal frequency ω by

$$\Omega = \omega/V_a \tag{59}$$

The wind gust velocities along the aircraft's body axes will be denoted by the subscript b. It is assumed that u_{g_b} is uncorrelated with both ω_{g_b} and q_{g_b}; but ω_{g_b} and q_{g_b} are correlated, since q_{g_b} is due to the variation of ω_{g_b} along the aircraft's body. Using Taylor's hypothesis of a "frozen field," [10], these spectra can be expressed in terms of the temporal frequency ω by

$$S_i(\omega) = \frac{1}{V_a} S_i(\frac{\omega}{V_a}), \quad i = u, \omega, q. \tag{60}$$

A mathematical model of the gusts can be obtained using spectral factorization [11], [12], [13].

1. Model of u'_{g_b} - Using (56), (60) and (51), the spectrum of u'_{g_b} can be found to be

$$S_{u'}(\omega) = \frac{2L_u\sigma_u^2}{V_a^3} \frac{1}{1 + (\frac{L_u}{V_a})^2 \omega^2} \tag{61}$$

$$= \frac{2L_u\sigma_u^2}{V_a^3} \frac{1}{1 - j\frac{L_u}{V_a}\omega} \frac{1}{1 + j\frac{L_u}{V_a}\omega}. \tag{62}$$

This corresponds to a system with transfer function $G_u(s)$ driven by a white noise with power $2L_u\sigma_u^2 / V_a^3 (ft^2/sec^2)/Hz$.

$$G_u(s) = \frac{1}{1 + \frac{L_u}{V_a} s} \tag{63}$$

2. Model of α_{g_b} - Using (57) and (60) the spectrum of α_g can be found to be

$$S_\alpha(\omega) = \sigma_\omega^2 \frac{L_\omega}{V_a^3} \frac{1 + 3(\frac{L_\omega}{V_a})^2 \omega^2}{\left[1 + (\frac{L_\omega}{V_a})^2 \omega^2\right]^2} \tag{64}$$

$$= \frac{\sigma_\omega^2 L_\omega}{V_a^3} \frac{1 - j\sqrt{3}\frac{L_\omega}{V_a}\omega}{\left(1 - j\frac{L_\omega}{V_a}\omega\right)^2} \frac{1 + j\sqrt{3}\frac{L_\omega}{V_a}\omega}{\left(1 + j\frac{L_\omega}{V_a}\omega\right)^2}. \tag{65}$$

From equation (65), it is seen that a system with transfer function $G_\alpha(s)$, given below, driven by white noise with power $\sigma_\omega^2 L_\omega / V_a^3 (ft^2/sec^2)/Hz$ generates the spectrum in (64).

$$G_\alpha(s) = \frac{1 + \sqrt{3}\,\frac{L_\omega}{V_a}\,s}{1 + 2\frac{L_\omega}{V_a}\,s + \left(\frac{L_\omega}{V_a}\right)^2 s^2} \tag{66}$$

3. Model of q_{g_b} - Using (58) and (60), the power spectral density of q_{g_b} can be found to be

$$S_q(\omega) = \frac{\omega^2}{1 + (\frac{4b}{\pi V_a})^2 \omega^2} \cdot S_\alpha(\omega) \tag{67}$$

$$= \frac{(-j\omega)}{1 - j\frac{4b}{\pi V_a}\omega} G_\alpha(-j\omega) \cdot \frac{(j\omega)}{1 + j\frac{4b}{\pi V_a}\omega} G_\alpha(j\omega) \,. \tag{68}$$

The cross-correlation of q_{g_b} and α_{g_b} is specified by their cross-spectral density

$$S_{q\alpha}(\omega) = \frac{j\omega}{1 + j\frac{4b}{\pi V_a}\omega} \; S_\alpha(\omega) \,. \tag{69}$$

From (68) and (69), it can be seen that if $\alpha_{g_b}(t)$ is input into the filter

$$G_q(s) = \frac{s}{1 + \frac{4b}{\pi V_a}\,s} \,, \tag{70}$$

then, both the power spectral density and the cross-spectral density requirements will be met. A block diagram for generating the wind gust velocities is given in Figure 3. The inputs $w_1(t)$ and $w_2(t)$ are uncorrelated gaussian white noise processes. It should be noted that to obtain a stationary process, an initial period for the settling of the transients due to unmatched initial conditions need be allowed or the initial conditions so chosen as to obtain a stationary process immediately. Otherwise, the process would be non-stationary for a time corresponding to a few time constants.

4. Models of u_s' and α_s - The steady winds can also be modeled by differential equations, i.e., by setting the derivative of the variable equal to zero, and the initial condition equal to the value of the steady wind. To allow for slow variations a forcing function with a small magnitude can be added. Thus, the steady components with respect to the earth-fixed axes are modeled as

$$\dot{u}_s' = w_3, \quad \dot{\alpha}_s = w_4 \; ; \; u_s'(0) = \frac{u_s(0)}{U_o} \; , \; \alpha_s(0) = \frac{\omega_o(0)}{U_o} \tag{71}$$

where $u_s(0)$ and $\omega_s(0)$ are the steady wind values, and w_3, w_4 are independent white noise processes with very small power. To obtain the total winds u_w' and α_w, the gust and steady components are first transformed into the stability axes and then added as shown in (51), (52).

Thus the wind vector w in (50) can be expressed as the output of a linear system. The transfer functions $G_u(s)$, $G_\alpha(s)$ and $G_q(s)$ can be expressed in differential equation form, and then these equations can be put into state variable form.

$$\dot{W} = A_w W + B_w \xi, \quad w = C_w W, \tag{72}$$

where A_w, B_w and C_w are given by

$$A_w = \begin{bmatrix} 0 & 1 & 0 & 0 & 0 & 0 \\ -\frac{V_a^2}{L_\omega^2} & -\frac{2V_a}{L\omega} & 0 & 0 & 0 & 0 \\ \frac{\pi V_a}{4b} & 0 & -\frac{\pi V_a}{4b} & 0 & 0 & 0 \\ 0 & 0 & 0 & -\frac{V_a}{L_u} & 0 & 0 \\ 0 & 0 & 0 & 0 & 0 & 0 \\ 0 & 0 & 0 & 0 & 0 & 0 \end{bmatrix}$$

$$B_w \begin{bmatrix} \sqrt{3}\,\frac{V_a}{L_\omega} & 0 & 0 & 0 \\ (1 - \sqrt{12})(\frac{V_a}{L_\omega})^2 & 0 & 0 & 0 \\ 0 & 0 & 0 & 0 \\ 0 & \frac{V_a}{L_\omega} & 0 & 0 \\ 0 & 0 & 1 & 0 \\ 0 & 0 & 0 & 1 \end{bmatrix}$$

$$C_w = \begin{bmatrix} -\sin\alpha_o & 0 & 0 & -\cos\alpha_o & -\cos(\sigma_o + \theta) & \sin(\sigma_o + \theta) \\ -\cos\alpha_o & 0 & 0 & \sin\alpha_o & -\sin(\sigma_o + \theta) & -\cos(\sigma_o + \theta) \\ -\frac{\pi V_a}{4b} & 0 & \frac{\pi V_a}{4b} & 0 & 0 & 0 \end{bmatrix}$$

Thus, equation (50) describes the aircraft's motion due to changes in the control variables and wind conditions, while (72) describes the statistical properties of wind gust velocities and steady winds. Hence, the aircraft's equations of motion have been expressed by a linear dynamical system of equations in state variable form.

C. Discretization of the Equations of Motion

In this section, the equation of motion given in (50) and the wind equations given in (72) are discretized; i.e., the differential equations (50), (72) are replaced by difference equations which update the state variables from one sampling instant to the next. There are two major reasons that lead to the discretization of the equations of motion. The first is due to the simulation of the aircraft's motion on a digital computer. Due to the nature of digital computers, the integration of the equations of motion has to be performed in a discrete manner. The second, and more important, reason is inherent in the operation of some of the components of the system. The aircraft's position is obtained from the Microwave Landing System (MLS) which provides this data at discrete intervals of time, rather than continuously. Furthermore, the aircraft's control system includes a digital computer to perform the operations required for the implementation of the control law. Thus, the control commands at the computer output are, of necessity, discrete. These considerations lead to the discretization of the equations of motion.

Let $t_k = K\bar{T}$ be the times at which the aircraft's state has to be known; then it is required that the state be updated from t_k to t_{k+1}. This can be done by integrating equation (50). The result is given by [14]:

$$x(t_{k+1}) = \phi(t_{k+1} - t_k)x(t_k) + \int_{t_k}^{t_{k+1}} \phi(t_{k+1} - s)Bu(s)ds + \int_{t_k}^{t_{k+1}} \phi(t_{k+1} - s)Dw(s)ds, \tag{73}$$

where $\phi(t)$ is the transition matrix of A; i.e. $\phi(t)$ is the matrix exponential e^{At}. Now, since the control law is digital, we shall assume that the control command does not vary over one sampling period, i.e.,

$$u(t) = u_k, \; t_k \leq t < t_{k+1}. \tag{74}$$

Using (74) and the change of variable

$$s = t_k + \tau$$

(73) can be expressed as

$$x(t_{k+1}) = \phi(T)x(t_k) + \left[\int_0^T \phi(T - \tau)d\tau B \right] u_k + \int_0^T \phi(T - \tau)Dw(t_k + \tau)d\tau. \tag{75}$$

Now, the wind equations (72) can be integrated in a similar manner to obtain:

$$W_{k+1} = \phi_w W_k + \xi_k, \; w_k = C_w W_k, \tag{76}$$

where w_k and W_k represent $w(t_k)$ and $W(t_k)$, respectively, and*

$$\phi_w = e^{A_w T}, \quad \xi_k = \int_0^T \phi_w(T - \tau)B_w \xi(t_k + \tau)d\tau. \tag{77}$$

It can be shown that $\{\xi_k\}$ is a white noise sequence [15], with covariance

$$R_\xi = E(\xi_k \xi_k') = \int_0^T \phi_w(T - \tau)B_w F B_w' \phi_w'(T - \tau)d\tau, \tag{78}$$

where $F\delta(t - s)$ is the covariance of the continuous white noise process $\xi(t)$. Now, note that

$$w(t_k + \tau) = C_w \phi_w(\tau)W_k + \int_0^T \phi_w(\tau - s)B_w \xi(t_k + s)ds. \tag{79}$$

After substituting (79) into (75) and some manipulation

$$x_{k+1} = \phi x_k + \Gamma u_k + \Gamma_w W_k + \eta_k, \tag{80}$$

where x_k represents $x(t_k)$, and

$$\phi = e^{AT}, \quad \Gamma = [\int_0^T \phi(T - s)ds]B, \Gamma_w = \int_0^T \phi(T - s)DC_w \phi_w(s)ds, \tag{81}$$

$$\eta_k = \int_0^T \left[\int_s^T \phi(T - \tau)DC_w \phi_w(\tau - s)d\tau \right] \xi(t_k + s)ds. \tag{82}$$

---

* The matrices A_w, B_w and C_w have been evaluated at the steady flight condition for these derivations.

It should be noted that $\{\eta_k\}$ is also a white noise sequence, and which includes those effects of the winds which are not correlated to W_k. Thus, equations (80) and (76) are the discrete versions of the aircraft equations of motion (50) and wind equations (72), respectively. These equations can be programmed on a digital computer to simulate the motion of the aircraft under various wind conditions, and in the development of a digital control law for glideslope capture.

III. Development of the Filter Equations

The aircraft position is obtained from the Microwave Landing System (MLS). This data is obtained at discrete intervals of time and with high accuracy. The discrete character of the data makes it suitable for digital processing. Since the data has a high accuracy, it is of interest to investigate the possibility of deriving the signal parameters used by the guidance and control system without the use of costly inertial navigation systems. This can be done by processing MLS data and other sensor outputs through a filter which estimates the desired parameters. Hence, in this section, the equations defining the filter processing will be developed using MLS data, air data and body mounted accelerometers without using inertial platform data. A discrete-time Kalman filter with constant coefficients to reduce the amount of on-board computation will be used for filtering purposes.

A. Development of Measurement Models

To describe the characteristics of the data obtained from various sensors, simple models which describe sensor errors statistically will be developed. Models for these measurements including the associated errors are required both for simulation and filtering developments. As a Kalman filter will be used for processing, the errors in the measurements will be described as additive for filter design purposes; however, when this is unrealistic a different model will be used for the simulation of the errors which are actually input to the filter. It will be assumed that the bias error in the measurements is either negligible or has been subtracted from the data; otherwise, a pre-filter should be included for that purpose. As this study considers the longitudinal

equations of motion, the measurements considered here are those which affect the longitudinal variables. The measurements considered and the associated source of the measurements are listed below.

Y_1 = pitch angle (gyro)

Y_2 = pitch rate (gyro)

Y_3 = slant range (MLS)

Y_4 = elevation angle (MLS)

Y_5 = altitude (barometric)

Y_6 = sink rate (barometric)

Y_7 = acceleration along z_s (body-mounted accelerometer)

Y_8 = true airspeed (air data computer)

Y_9 = acceleration along x_s (body-mounted accelerometer)

The sensor models used for the simulation of the measurements are given below.

$$Y_1 = \Theta_o + \theta + \nu_1 = \Theta_o + x_1 + V_1 \tag{83a}$$

$$Y_2 = \dot{\theta} - \nu_2 = x_4 + V_2 \tag{83b}$$

$$Y_3 = [(U_o x_5 + x_o - x_a)^2 + (U_o x_6 + z_o - z_a)^2]^{1/2} + V_3 \tag{83c}$$

$$Y_4 = \tan^{-1}\left(\frac{U_o x_6 + z_o - z_e}{U_o x_5 + x_o}\right) + V_4 \tag{83d}$$

$$Y_5 = -(U_o x_6 + z_o + V_5) \tag{83e}$$

$$Y_6 = -(U_o \dot{x}_6 + \dot{z}_o)V_6 \tag{83f}$$

$$Y_7 = U_o[\dot{x}_2 \tan x_3 + \frac{1 + x_2}{\cos^2 x_3}\dot{x}_3 - x_4(1 + x_2 + \cos x_1 - \cos x_3)] + V_7 \tag{83g}$$

$$Y_8 = U_o\left(\frac{1 + u'}{\cos\alpha}\right)V_8 \tag{83h}$$

$$Y_9 = U_o[\dot{x}_2 + (1 + x_2)x_4 \tan x_3 + \dot{x}_3 \sin x_3 - x_4 \sin x_1] + V_9 \tag{83i}$$

where x_o and z_o are the 4D coordinates of the desired glideslope at a given time, x_i for $i \geq 1$ is the i^{th} component of the state vector x given in (50), z_e is the vertical coordinate of the elevation antenna, x_a, z_a are the coordinates of the azimuth antenna and V_i is the noise introduced by the sensor. The expressions for the accelerations in Y_7 and Y_9 are obtained by writing the inertial velocities along the x_e and z_e axes in terms of the state variables, differentiating with respect to time and then transforming these accelerations to the stability axes, x_s, z_s. The earth-fixed coordinate system is referenced with respect to a point on runway centerline corresponding to the position of the elevation 1 antenna. The values for the standard deviations of the sensor noises were chosen to reflect current instrumentation standards [16], [17]; these are shown in Table 1.

To use these measurements as input to the Kalman filter it is necessary to express them as linear combinations of the aircraft state

variables x and wind variables W with additive noise. To achieve this a pre-filter processor is used. This processor is nonlinear and consists of a general coordinate transformation to obtain the variables suitable for filtering. The equations describing the processing performed are given below.

$$r_e = [Y_3^2 - L_e^2 \quad 2L_e Y_3 \cos(Y_4 + \eta)]^{1/2}, \eta = \tan^{-1} \frac{h_{ea}}{x_a} \tag{84}$$

$$y_1 = Y_1 - \theta_o = x_1 + \nu_1 \tag{85a}$$

$$y_2 = Y_2 = x_4 + \nu_2 \tag{85b}$$

$$y_3 = \frac{-1}{U_o} [r_e \cos Y_4 + x_o] = x_5 + \nu_3 \tag{85c}$$

$$y_4 = \frac{-1}{U_o} [r_e \sin Y_4 - z_e + z_o] = x_6 + \nu_4 \tag{85d}$$

$$y_5 = \frac{1}{U_o} [z_o - Y_5] = x_6 + \nu_5 \tag{85e}$$

$$y_6 = \frac{1}{U_o} [\sin\gamma_o - Y_6] = \varepsilon_6' Ax + \nu_6. \tag{85f}$$

$$y_7 = \frac{Y_7}{U_o} - \varepsilon_3' Bu = \varepsilon_3'(Ax + DC_w W) + \nu_7 \tag{85g}$$

$$y_8 = \frac{Y_8}{U_o} - 1 = x_2 - \varepsilon_1' C_w W + \nu_8 \tag{86h}$$

$$y_9 = \frac{Y_9}{U_o} = \varepsilon_2'(Ax + DC_w W) + \nu_9 \tag{85i}$$

where h_{ea} is the height of the elevation antenna above the azimuth antenna, x_a is the distance of the Az. antenna from the origin, L_e is given by $(x_a/\cos\eta)$, r_e is the range from the elevation antenna, ε_j is a column vector equal to the j^{th} column of the identity matrix and v_j is a pseudo noise representing the additive noise in the processed measurement vector y. The first equality in (85) gives the processing done to obtain y from the total measurements Y, while the second equality (i.e. the right hand side of (85)) provides the measurement model which is used in the development of the filter. This model can be written in matrix form as

$$y(t_k) = y_k = C_1 x_k + C_2 W_k + v_k, \tag{86}$$

where C_1 and C_2 correspond to the appropriate coefficients given in the second equality of (85). Thus, a mathematical model to simulate the noisy measurements Y, a nonlinear processor and a linear measurement model with additive noise for the development of a Kalman filter are obtained.

B. Development of Filter Equations

The output of the pre-filter processor, y_k, given in (86) can be used as the input to the filter. In turn, the filter reduces the noise introduced by the sensors by optimally weighing new data versus previous estimates and also generates estimates of variables which are not directly measured using the equations by which the dynamical system is governed. The variables which are not directly measured include the

angle of attack and the wind velocities; thus the filter output provides optimal estimates of all the state variables and the wind velocities. The control system uses these estimates to calculate the control surface settings thus closing the loop around the aircraft viewed as a dynamical system.

Since estimates of the wind velocities as well as the aircraft state variables are to be obtained, it is desirable to combine the aircraft equations of motion (80), and the wind model (76) into a single system of equations. Thus, let

$$X_k' = (x_k' \quad W_k') \ , \quad \zeta_k' = (\eta_k' \quad \xi_k') \ , \tag{87a}$$

$$\alpha = \begin{pmatrix} \phi & \Gamma_w \\ 0 & \phi_w \end{pmatrix} \ , \quad \beta = \begin{pmatrix} \Gamma \\ 0 \end{pmatrix} \ , \quad C = (C_1 \quad C_2) \tag{87b}$$

In this notation (80), (76) and (86) can be written as

$$X_{k+1} = \alpha X_k + \beta u_k + \zeta_k, \ y_k = CX_k + \nu_k \ . \tag{88}$$

Now, it is desired to obtain estimates, $\hat{X}_k$, of X_k using the available measurements y_k. A Kalman filter for the system given in (88) would provide optimal estimates of X_k. Note that, whatever processing is done by the filter, it will require a certain amount of time on a digital computer; thus the estimates will be available for use by the control system only after the filtering computations have been performed. It is known that such delays in the control loop can lead

to instability [18] in digital control systems if they are not compensated. Thus it is desirable to obtain estimates with minimum delay. This can be accomplished by predicting X_k from the past measurements y_{k-1}, y_{k-2}, ...; i.e. without using the present measurement y_k. In this way, at time t_{k-1} the measurements y_{k-1} are obtained and the computations necessary to obtain $\hat{X}_k$ are initiated. If these computations can be performed in less than one sampling period, T, then $\hat{X}_k$ is available at time t_k. Hence, a one-step predictor algorithm is best suited for this application. The optimal prediction algorithms for the system given by (88) are the well-known Kalman equations [19], [20], [21].

$$\hat{X}_{k+1} = \alpha\hat{X}_k + \beta u_k + G_k(y_k - C\hat{X}_k), \tag{89a}$$

$$P_{k+1} = \alpha P_k \alpha' - \alpha P_k C'[CP_kC' + R_k]^{-1} CP_k\alpha' + Q_k , \tag{89b}$$

$$G_k = \alpha P_k C'[CP_kC' + R_k]^{-1} \tag{89c}$$

where P_k is the covariance of the error, $X_k - \hat{X}_k$, and the measurement and state noise covariances are given by

$$E(\zeta_k \ \zeta_j') = Q_k\delta_{kj} , \quad E(\nu_k \ \nu_j') = R_k\delta_{kj}. \tag{90}$$

Note that (89a) is a predictor algorithm since it uses u_k which is available at time t_k to compute $\hat{X}_{k+1}$ which is not used until t_{k+1}; (89b) propagates the error covariance and (89c) gives the filter gain matrix.

It is important to note that to update the estimates recursively as shown in (89a) only the gain matrix G_k is needed.

It is well-known that if the noise covariances Q_k and R_k do not depend on time, i.e.,

$$Q_k \equiv Q, \quad R_k \equiv R, \text{ for all } k \tag{91}$$

then the solution P_k of the matrix equation of Riccati type given by (89b) converges to a steady state error covariance, say P, for a broad class of dynamical systems (α,β,C). The observability of (α,C) is a sufficient but not necessary condition for the convergence of P_k; a necessary and sufficient condition is given in [21]. Thus, in the steady state situation, the gain G_k also converges to a corresponding value, say G, given by (89c). Hence, the filter (89a) becomes a time-invariant system. The implications of this convergence to the implementation of the filter are that the error covariance equation (89b) can be solved off-line and the steady state gain G can be computed prior to flight; so that the only computations which need to be performed in real time, i.e. during flight, are the operations described by (89a). As the propagation of the error covariance generally requires a very large number of computations compared to the update of the estimates, the use of the steady state gain reduces the number of operations that need to be performed on-line considerably. The reduction in computation time thus gained may allow the use of a sophisticated model for the aircraft dynamics, thus increasing the accuracy of the estimates. The number

of computations required can further be decreased by taking advantage of the special properties of the matrices involved. However, for the most general case where no special properties are present, the number of multiply-add operations required to update the estimates from one sample to the next is roughly given by $n(n + p + 2m)$, where n is the number of variables which are estimated (i.e. the dimension of X_k), p is the number of control variables (i.e. the dimension of u_k) and m is the number of measurements.

In this study, the steady state gains were used to take advantage of the reduction in the number of on-line computations required. If no advantage of the special form of α and β is taken, the number of multiply-add operations required is 646 per update. Taking advantage of the form of α and β as given in (87b) this number can be reduced to 468. Further substantial reductions are possible using the properties of ϕ, ϕ_w, C_1 and C_2; however these were not investigated in this study. If new estimates are required at a rate of ten per second, the above computations would require that one multiply-add operation be performed in a maximum period of 200 μsec, including memory access time. Simulations of the filter under various conditions were done. Plots of these runs are shown in Figures 6 - 12; these are discussed in Section V. A block diagram of the filter is given in Figure 4.

IV. Development of Digital Automatic Control Law

During the final approach phase, the aircraft aligns itself with the runway during localizer capture and stabilizes on a straight and level course, it remains on this course until the glideslope capture maneuver starts, then follows the glideslope until the flare maneuver brings it to touchdown. Thus, as the aircraft starts to capture the glideslope its control surfaces are set so as to follow a constant altitude straight line flight path. Hence, the function of the control law to be developed is to take the aircraft from this condition to another steady condition with a constant sink rate and follow the flight path defined by the glideslope in an automatic mode using a digital computer for the control law computations. In terms of the aircraft equations of motion given by (50), this corresponds to starting from an initial state that describes a constant speed level flight condition and bringing the state variables x to a value as close to zero as allowed by the wind conditions. As the state vector x represents the deviation of the aircraft longitudinal variables from their value on the glideslope, a value of zero for x means no deviation from the desired flight path. As the winds, however, will cause deviations from this flight path, it is necessary for the control law to take action against deviations caused by random wind gusts. These objectives can be mathematically described by a quadratic cost function that penalizes more for large values of x (i.e. large deviations from the glideslope) than values close to zero:

$$J(u) = \frac{1}{2} E \int_{t_o}^{t_f} [x'(t)\bar{Q}x(t) + u'(t)\bar{R}u(t)]dt, \qquad (92)$$

where $\bar{Q}$ and $\bar{R}$ are non-negative definite matrices chosen so as to reflect the relative importance of deviations in the state variables and controls from their desired values and E denotes the statistical expectation operator. Thus, a control law is judged depending on the value of the cost function J(u); a small value for J(u) corresponds to small deviations from the glideslope, hence to a "good" control law. Thus, it is desirable to find a control law for which the cost function is minimum or at least small.

A. Discretization of the Cost Function

The aircraft equations of motion (50) and the wind model (72) were discretized in Section IIC. The cost function (92) can also be discretized [15] under the assumptions that the measurement noise $\{\nu_k\}$ and the wind generation noise $\{\xi_k\}$ have zero mean and are gaussian, and that the control u(t) remains constant over each sampling period, i.e., equation (74) holds. If the cost function is discretized then the optimal control problem of minimizing J(u) under the constraints of (80) and (76) can be solved using dynamic programming.

First note that (92) can be broken down to a sum of terms by integrating over each sampling period.

$$J(u) = \frac{1}{2} E \sum_{k=0}^{M} \int_{t_k}^{t_{k+1}} [x'(t)\bar{Q}x(t) + u'(t)\bar{R}u(t)]dt. \qquad (93)$$

Now, using (50) and (72), and x(t) and W(t) can be expressed as

$$x(t_k + s) = \phi(s)x(t_k) + \Gamma_w(s)W(t_k) + \Gamma(s)u_k + n_k(s) \tag{94a}$$

$$W(t_k + s) = \phi_w(s)W(t_k) + \xi_k(s), \quad 0 \le s \le T, \tag{94b}$$

where $\phi(s)$ and $\phi_w(s)$ are the matrix exponentials e^{As} and $e^{A_w s}$, respectively, and

$$\Gamma(s) = [\int_0^s \phi(s - \tau)d\tau]B, \; \Gamma_w(s) = \int_0^s \phi(s - \tau)DC_w\phi_w(\tau)d\tau, \tag{95a}$$

$$n_k(s) = \int_0^s \left[\int_\tau^s \phi(s - \tau')DC_w\phi_w(\tau' - \tau)d\tau' \right] \xi(t_k + \tau)d\tau, \tag{95b}$$

$$\xi_k(s) = \int_0^s \phi_w(s - \tau)\xi(t_k + \tau)d\tau. \tag{95c}$$

Note that $x(t_k)$, $W(t_k)$, $\Gamma(T)$, $\Gamma_w(T)$, $\phi(T)$, $\phi_w(T)$, $\eta_k(T)$ and $\xi_k(T)$ correspond to x_k, W_k, Γ, Γ_w, ϕ, ϕ_w, η_k and ξ_k, respectively, in previous notation. The above expressions for $x(t_k + s)$ and $W(t_k + s)$ can be substituted into a general term of the summation in (93), after some manipulation we obtain

$$E\int_{t_k}^{t_{k+1}} [x'(t)\bar{Q}x(t) + u'(t)\bar{R}u(t)]dt = E\int_0^T [x'(t_k + s)\bar{Q}x(t_k + s) + u'(t_k + s)\bar{R}u(t_k + s)]ds \tag{96a}$$

$$= E[x_k'\hat{Q}x_k + 2x_k'NW_k + 2x_k'Mu_k + 2W_k'Su_k + u_k'\hat{R}u_k] + c_k^2, \tag{96b}$$

where

$$\hat{Q} = \int_0^T \phi'(\tau)\bar{Q}\phi(\tau)d\tau, \tag{97a}$$

$$M = \int_0^T \phi'(\tau)\bar{Q}\Gamma(\tau)d\tau, \tag{97b}$$

$$N = \int_0^T \phi'(\tau)\bar{Q}\Gamma_w(\tau)d\tau, \tag{97c}$$

$$S = \int_0^T \Gamma_w'(\tau)\bar{Q}\Gamma(\tau)d\tau, \tag{97d}$$

$$\hat{R} = \int_0^T \Gamma'(\tau)\bar{Q}\Gamma(\tau)d\tau + T\bar{R}, \tag{97e}$$

and c_k^2 is a constant depending only on the covariance of the white noise process $\xi(t)$. It should be noted that $\eta_k(s)$ and $\xi_k(s)$ depend only on the values of $\xi(t)$ which occur after t_k; this can be seen from (95b) and (95c). On the other hand x_k and W_k depend on the values of $\xi(t)$ before t_k. Since $\xi(t)$ is a zero mean gaussian white noise process, its values before t_k and those after t_k are independent; thus,

$$E(x_k\eta_k'(s)) = E(x_k\xi_k'(s)) = E(W_k\eta_k'(s)) = E(W_k\xi_k'(s)) = 0 \tag{98}$$

Hence, the terms in (96a) which involve the cross-correlations in (98) do not influence the discrete cost function (96b). On the other hand, note that c_k^2 does not depend on the values of the u_k. Thus, it does not affect the minimization of the discrete cost function with respect to u_k

and can be ignored. The above result is summarized in the following lemma.

Lemma 1 The cost function J given by (93) and the discrete costs function J_1 given below differ by a constant independent of u_k, hence, J and J_1 are equivalent as far as minimization with respect to u_k is concerned.

$$J_1(u) = \frac{1}{2} E \sum_{k=0}^{M} (x_k'\hat{Q}x_k + 2x_k'NW_k + 2x_k'Mu_k + 2W_k'Su_k + u_k'\hat{R}u_k) \qquad (99)$$

Thus, the continuous cost function can be expressed in terms of the samples of the variables at the sampling instants, t_k. Note that (99) contains cross product terms between the aircraft variables x_k and the wind velocities W_k and the controls u_k, whereas the continuous cost function contains no cross product terms. It can be seen from (97) that the cross terms as well as the quadratic terms represent the effect of the dynamics in between sampling instants. As the system response between the sampling instants is included in the discrete cost function, it becomes possible to use sampling periods larger than generally used, thus allowing more time for computation during updates of the estimates and the control.

B. Solution of the Optimal Control Problem

The optimal control problem of minimizing a quadratic cost function with the constraint of a linear dynamical system with gaussian statistics has been extensively treated in the literature [22 and the references therein]. The problem considered here differs from the usual one in two

ways; the cost function contains cross products terms as mentioned in the previous section and the state of the system is affected by a random disturbance which can be described by linear dynamics; i.e. the disturbance is not white noise. The case of non-random disturbances was treated in [23], [24], [25]. The problem considered here is also treated in [26].

Consider the optimal sampled-data control problem posed by the aircraft dynamics (50), the wind model (72), the control constraint (74), the discrete measurement equations (85) and the costs function (93). In earlier sections this sampled-data problem has been reduced to a discrete form with the discrete aircraft equations described by (80), the wind model by (76), the measurements by (85) and the cost function by (99). Thus, the optimal control problem is reduced to minimizing the cost function (99) with respect to the control sequence $\{u_k\}$, where u_k is restricted to depend only on the past measurements $\{y_i,\ 0 \le i \le k-1\}$ as these measurements only are available for controlling the aircraft.*

To derive the control u_k which minimizes the cost function (99) the dynamic programming method [27] will be used. Thus, consider a general term in (99).

$$I_k(u_k) = \frac{1}{2} E[x'_{k+1} P_{1k} x_{k+1} + 2x'_{k+1} P_{2k} W_{k+1} + 2x'_k M u_k + 2W'_k S u_k + u'_k \hat{R} u_k] \tag{100}$$

* This restriction is mathematically interpreted as: u_k is measurable with respect to the σ-algebra generated by the random variables $\{y_i,\ 0 \le i \le k-1\}$.

Note that as $E(x_o'\hat{Q}x_o)$ and $E(x_o'NW_o)$ are constants they can be excluded from the minimization, so that the general term in (99) can be written as shown in (100). Now, substituting (80) and (76) into (100) and regrouping terms

$$I_k(u_k) = \frac{1}{2} E[x_k'\phi P_{1k}\phi x_k + 2x_k'\phi' D_k W_k + 2u_k' G_{1k} x_k + 2u_k' G_{2k} W_k + u_k'\hat{R}_k u_k] + d_k, \tag{101}$$

where

$$D_k \equiv P_{1k}\Gamma_w + P_{2k}\phi_w, \quad \hat{R}_k \equiv \hat{R} + \Gamma' P_{1k}\Gamma, \tag{102a}$$

$$G_{1k} = \Gamma' P_{1k}\phi + M, \quad G_{2k} \equiv \Gamma' D_k + S, \tag{102b}$$

$$d_k = \frac{1}{2} E(W_k'\Gamma_w' D_k W_k + \eta_k' P_{1k}\eta_k + \eta_k' P_{2k}\xi_k). \tag{102c}$$

First note that the cross-correlations of x_k, W_k u_k with η_k or ξ_k are zero as shown in (98), and

$$E(u_k\eta_k') = E(E(u_k\eta_k'|y_k)) = E(u_k E(\eta_k'|y_k)) = 0^*, \tag{103}$$

and similarly for $E(u_k \quad \xi_k')$; so that these terms have been dropped from (101). Also note that d_k depends only on the statistics of the

---

* y_k is the σ-algebra generated by the past measurements $\{y_i,\ 0 \le i \le k-1\}$, [5].

disturbances (i.e. winds), but does not vary with the control sequence. Now, note that since u_k depends only on past measurements, using a well-known lemma on conditional expectations [8],

$$E(u_k'G_{1k}x_k) = E(E(u_k'G_{1k}x_k|y_k)) = E(u_k'G_{1k}\hat{x}_k) \tag{104a}$$

$$E(u_k'G_{2k}W_k) = E(u_k'G_{2k}\hat{W}_k), \tag{104b}$$

where $\hat{x}_k$ and $\hat{W}_k$ are the conditional expectations $E(x_k|y_k)$, $E(W_k|y_k)$ respectively. Note that $\hat{x}_k$ and $\hat{W}_k$ are the components of $\hat{X}_k$ in (89) so that $\hat{x}_k$ and $\hat{W}_k$ are obtained from the filter output. Substituting (104) into (101),

$$I_k(u_k) = \frac{1}{2} E[x_k'\phi'P_{1k}\phi x_k + 2x_k'\phi'D_kW_k + 2u_k'(G_{1k}\hat{x}_k + G_{2k}\hat{W}_k) + u_k'\hat{R}_1u_k] + d_k. \tag{105}$$

Minimization of I_k with respect to u_k results in

$$u_k = -\hat{R}_k^{-1}[G_{1k}\hat{x}_k + G_{2k}\hat{W}_k], \text{ a.e.} \tag{106}$$

Note that since $\hat{x}_k$ and $\hat{W}_k$ depend only on the past measurement, so does u_k, and the restriction on u_k is thus satisfied by (106). Now, substituting (106) into (105) and adding the next general term in (99), we obtain

$$I_{k-1}(u_{k-1}) = \frac{1}{2} E[x_k' P_{1k-1} x_k + 2x_k' P_{2k-1} W_k + 2x_{k-1}' M_{uk-1} + 2W_{k-1}' S u_{k-1} + u_{k-1}' \hat{R} u_{k-1}] + e_{k-1}, \tag{107}$$

where

$$P_{1k-1} \triangleq \phi' P_{1k} \phi - G_{1k}' \hat{R}_k^{-1} G_{1k} + \hat{Q}, \; P_{1M} = \hat{Q} \tag{108a}$$

$$P_{2k-1} = [\phi - \Gamma \hat{R}_k^{-1} G_{1k}]' D_k + N, \; P_{2M} = N \tag{108b}$$

$$e_{k-1} = d_k + \frac{1}{2} E[\hat{W}_k' G_{2k}' \hat{R}_k^{-1} G_{2k} \hat{W}_k + \tilde{x}_k' G_{1k}' \hat{R}_k^{-1} G_{1k} \tilde{x}_k + 2\tilde{x}_k' G_{1k}' \hat{R}_k^{-1} G_{2k} \tilde{W}_k] \tag{109a}$$

$$\tilde{x}_k = x_k - \hat{x}_k \; , \; \tilde{W}_k = W_k - \hat{W}_k. \tag{109b}$$

Since, W_k and x_k are gaussian random variables, it is known that [21] $E(\tilde{x}_k \tilde{x}_k')$, $E(\tilde{x}_k \tilde{W}_k')$ and $E(\tilde{W}_k \tilde{W}_k')$ do not depend on the value of u_k; hence, e_{k-1} is constant as far as minimization with respect to u_i. Since, (107) is of the same form as (100) except for a constant, the above steps can be applied to I_{k-1}, and continue the iteration until I_o is obtained. Hence, the following theorem summarized the result obtained.

Theorem 1 The optimal control problem posed by (50), (72), (74), (85) and (93) has a unique solution (a.e.) which is given by (106), (108) and (102),

$$u_k = -(\hat{R}_k^{-1}G_{1k})\hat{x}_k - (\hat{R}_k^{-1}G_{2k})\hat{W}_k = -H_{1k}\hat{x}_k - H_{2k}\hat{W}_k. \qquad (110)$$

The control is seen to consist of two parts. One uses the aircraft state estimates for feedback; note that the gain associated with this term is the same gain as the case when no disturbance is present. Thus this term accomplishes the stability about the glideslope to be followed; i.e., if the aircraft is not on the glideslope, its effect will be to bring the aircraft back on the glideslope. The second term uses the disturbance estimates; it acts as a preventive measure so that if a disturbance that will throw the aircraft off the glideslope is estimated by W_k, corrective control action will be taken before the aircraft is off the glideslope, and thus prevent flight path effors as much as possible before they occur.

C. Constant Feedback Gains

From the expression (11) for the control, it is seen that the feedback gains H_{1k} and H_{2k} vary with time, i.e. with k. Implementation of this control law would require solving the equations (108), (102) backwards, starting at K ▫ M, to determine the gains at each sampling instant, then storing these gains on an on-board computer to use them in the computation of the control. This would place a great burden on the computer's memory capacity and speed. The use of these time varying gains, however, is not necessary to obtain a good performance and stability. It is possible to use constant values for the feedback gains H_{1k} and H_{2k}, thus avoiding implementation complexity. In fact, with the use of constant gains to determine the control in (11), the control computations require

very little complexity in the on board computer. In this case, it is necessary to store the elements of H_1 and H_2 and compute (11) within a time period T, i.e. the sampling period. For the system considered here, the number of elements in H_1 and H_2 is 45, and the number of multiply-add operations required for each update of the control is 45. Thus, the control computations can be easily implemented on an on board computer.

To compute the constant gains to be used, it is necessary to solve equations (108) and (102) backward. It is known that P_{1k} converges to a steady value under very loose conditions [21], which are satisfied by the aircraft equations (50). The convergence of P_{2k} when ϕ_w has unstable poles is not always guaranteed. The following theorem given here without proof specifies necessary and sufficient conditions for the convergence of P_{2k}. Let $\rho(\phi)$ denote the largest of the absolute values of the eigenvalues of ϕ.

Theorem 2 Let P_{1k} converge. Then P_{2k} given by (108) converges if, and only if,

$$\rho(\phi - \Gamma H_1)\rho(\phi_w) < 1$$

Thus, the convergence of P_{2k} and H_2k depends on the degree of instability in the disturbance model. For the wind model considered here $\rho(\phi_w)$ has a value of 1, while $\rho(\phi - \Gamma H_1)$ is less than 1. Hence, the above condition is satisfied, and P_{2k}, H_{2k} both converge. The steady value of P_{2k} and the gain H_{2k} can be computed from (108) and (102).

The steady state value of P_{1k} was computed using a non-iterative approach [28]; i.e., the steady state value, say P_1, was computed without using (108a) which requires a large number of iterations to converge. In any case, this computation would be done off-line and place no real-time requirements. The steady state value of P_{2k} was also computed using a non-iterative method, developed by the author, which will not be given here. This method also reduced off-line computation time. Then, the gains H_1 and H_2 were determined using (11) and (102b). These gains were stored and used in the simulation of the control system. To avoid extremely high control commands which might be caused by component or sensor failures and would place high stress on the control surfaces limiters were placed as shown in Figure 5. Note that the stabilizer and throttle commands (u_{2k}, u_{3k}) are rate commands. If the stabilizer and throttle positions are needed, a hold circuit followed by an integrator can be used.

V. Results

Using the models developed in the earlier sections a versatile digital computer simulation was developed. The filter and the control law developed for the capture of a steep 6° glideslope were simulated on a digital computer. The aircraft equations of motion, linearized about a 6° glideslope developed in Section II.A and discretized for simulation in Section II.C, were coded on a digital computer to simulate the motion of the aircraft. The wind model developed in Section II.B was used to generate random gusts as well as steady winds to simulate the wind conditions for the simulation of a given flight. The MLS receiver outputs and on board sensor outputs were simulated by corrupting the position, velocity and attitude of the aircraft by noises characteristic of present day sensor errors, the models for these sensor errors are given in Section III.A. Thus, the simulation developed included the following:

1. aircraft motion in the longitudinal axis
2. wind conditions (gusts and steady winds)
3. sensor errors
4. filter
5. control law

Major parameters such as turbulence levels, steady winds were left as input variables in the simulation developed to allow for versatility of use. Thus, to simulate the aircraft motion under different wind conditions it is only necessary to specify the values of the wind gust and steady wind velocity parameters. The major parameters that can be specified include:

1. the standard deviations of wind gusts
2. scale of turbulence
3. steady wind velocities
4. standard deviations of the noises of each sensor and MLS
5. initial conditions at the start of glideslope capture
6. sampling rate, T

Note that by varying the sampling rate, T, it is possible to simulate varying rates for the reception of MLS data; by varying the noises on the various sensors, it is possible to degrade the quality of the MLS signal by adding noise to it and similarly for the other sensors.

A constant gain Kalman filter was developed to filter out the noise present in the various sensor outputs and to obtain estimates of various unmeasured parameters, such as wind velocities, and angle of attack. The filter combines position data from the MLS with air data from on-board sensors, body-mounted accelerometer data and aircraft attitude for this purpose. The estimates output by the filter are used to compute the control commands. The simulation runs made under varying wind conditions indicate that the estimates supplied by this filter follow the actual aircraft parameters with little error.

A digital automatic control law for the longitudinal axis to capture and follow a 6° glideslope was developed. The design procedure used was the general quadratic regulator theory with the modifications described in Chapter IV. The control law uses constant gains in the feedback loop, and also uses wind velocity estimates provided by the filter to retrim the aircraft and reduce the deviations caused by the

wind gusts. The 4D aspect of the control law is due to the fact that the position error fed back is the difference between the actual aircraft position and its desired position at each instant of time. Thus, the aircraft control law tries to bring the aircraft to a specified position at a specified time. The control law was simulated under various wind conditions and from different initial conditions as shown in Figures 6 - 12. The 4D errors in position, errors in sink rate and inertial speed are shown in the various plots. The performance of the aircraft in capturing a steep 6° glideslope from level flight at 120 knots appears to be acceptable.

Various simulation runs for capture and glideslope following are shown in Figures 6 - 12. The initial conditions corresponding to time zero, 30,000 ft. from the runway and an altitude of about 3,153 ft. have been specified as the beginning of the capture mode; i.e. at time zero the aircraft is trimmed for level flight at 120 knots (202.536 ft/sec); the capture mode is switched on when the aircraft's estimated altitude below the glideslope is 45 ft. Thus, the initial 4D vertical error shown in the simulation plots is not interpreted as an error but as a starting point from which the glideslope is to be acquired. Similarly, the initial conditions for pitch, sink rate, thrust, stabilizer, etc. are at the values required for level flight. The units used in the plots are ft. for distances, ft/sec. for velocities, degrees for angles, degrees per second for angular rates and seconds for time. Thrust is expressed in pounds, throttle in degrees (on the stick), elevator, and stabilizer in degrees. During the initial capture period, the

aircraft acquires the 6° glideslope by retrimming the stabilizer position, while the thrust is reduced. The elevator initiates the pitch-down motion, necessary to acquire a sink rate ($\dot{h}$) of about 21 ft/sec. The settling time for pitch, pitch rate, sink rate is about 10 seconds, while the position errors and speed take longer to reach their steady values. No extreme values are required for the controls during capture, and overshoots are not excessive although, in comparison to the usual 3° capture, the 6° capture is a relatively large change in flight condition.

To compare the effects of various levels of wind gusts, steady winds and sensor errors, the hypothetical case of no sensor noise and no wind was simulated (Figure 6). The aircraft motion for this case is smooth, and after capture the deviations from the glideslope settle to zero. The introduction of sensor noise on the measurements (Fig. 7) causes slight but noticeable deviations from the glideslope in all the variables; this is caused through the errors in the estimates of the aircraft variables due to imperfect measurments. The effects of wind gusts on the aircraft response can be seen in Figures 8 - 10. The turbulence levels are specified through the standard deviation of longitudinal gust velocities, σ_u, and the vertical gust velocities, σ_w. As can be seen from the plots, the wind gusts affect the aircraft motion considerably. The control action increases in order to reduce the flight path deviations from the glideslope by using the proper feedback. The maximum deviations while following the glideslope are within acceptable limits in the various wind conditions. It should be noted that these deviations could be further reduced by allowing a higher level of control activity.

This can be achieved simply by reducing the value of the elements of $\bar{R}$ in the cost function (92). To see the effect of a higher sampling rate on the performance of the aircraft motion, a rate of 10 per second instead of 5 per second was used for incoming data and control commands. This case is shown in Fig. 12; a slightly tighter performance in the aircraft deviations can be seen; however, the basic response characteristics are the same. It should be noted, however, that even though rates of 5 per second appear to be satisfactory for glideslope capture, the flare maneuver may require a higher rate. In general, the control law appears to be performing satisfactorily during the glideslope capture and glideslope following phases of final approach.

The various plots with sensor noise and wind gusts show that the constant gain filter tracks the various parameters with considerable accuracy. The case for no wind and no measurement error (Fig. 6) is given as a reference for comparison of the effects of inducing sensor noise and winds of various magnitudes. The case of no measurement noise (Fig. 6) shows no noticeable error in the estimates, as would be expected. When measurement noise is introduced (Fig. 7) errors in the estimates become noticeable. When wind gusts are introduced (Fig. 8), the errors in the estimates increase slightly; however, this increase in the errors is small in comparison to the errors due to sensor noise (Fig. 7). Also note that the wind velocities are estimated with accuracy, the measurements containing information about wind velocities are airspeed and the accelerations; these appear to be sufficient to track the wind velocities. Steady winds are also estimated with accuracy

as can be seen in Fig. 9. Figure 11 shows a case where the initial values of the estimates are different than the actual values. In general, it can be said that the constant gain Kalman filter has a satisfactory performance in filtering sensor noises out and providing estimates of unmeasured variables.

VI. Conclusions

In the previous sections a digital automatic control law for steep glideslope capture and glideslope tracking was developed. The control law consists of a filter and a controller. The filter accepts MLS data, air data, attitude data and body-mounted accelerometer data, filters out the sensor noise in the measurements and outputs estimates of the measured variables, aircraft velocities and wind velocities. The controller uses these estimates to compute surface setting commands. A digital computer simulation of the aircraft motion, sensor noises, wind conditions, the filter and the controller has been developed to test the concepts used in the development of the overall control law for automatic steep glideslope capture and tracking. On the basis of the simulation results, the use of steep glideslopes during the glideslope capture and glideslope tracking phases of the final approach appears to be feasible.

For the filter concept used in this study, the use of costly inertial platform data can be replaced by less costly body-mounted accelerometer data (which have less accuracy) to obtain sufficiently accurate estimates of the variables needed for control purposes. It may be possible to eliminate the use of accelerometer data using this type filter as long as accurate MLS data is available; however, as inexpensive accelerometers are available, this case was not considered here. Further research is required to determine if the accuracy of velocity and acceleration estimates obtained using only MLS data would be sufficient for successful automatic landing under turbulence. The

simulation results also indicate that the concepts used in the development of the control law can provide successful control action for steep glideslope capture and tracking under various levels of turbulence.

Another critical phase of the final approach to landing is the flare maneuver. During a steep approach, due to larger changes in pitch and sink rate required, the flare maneuver is more critical than for shallower approaches. Thus, further research to investigate the problems which may be encountered in flare during a steep approach would be required for a complete evaluation of steep approaches to landing.

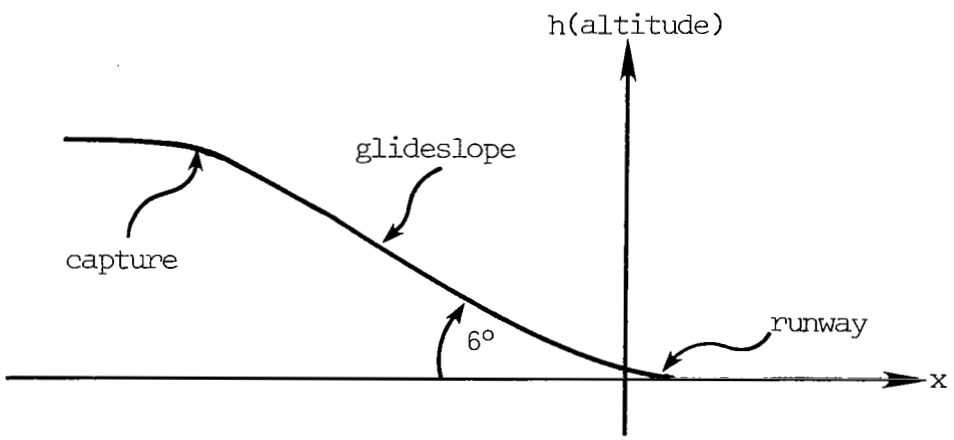

Figure 1 Flight Path for Capture and Glideslope

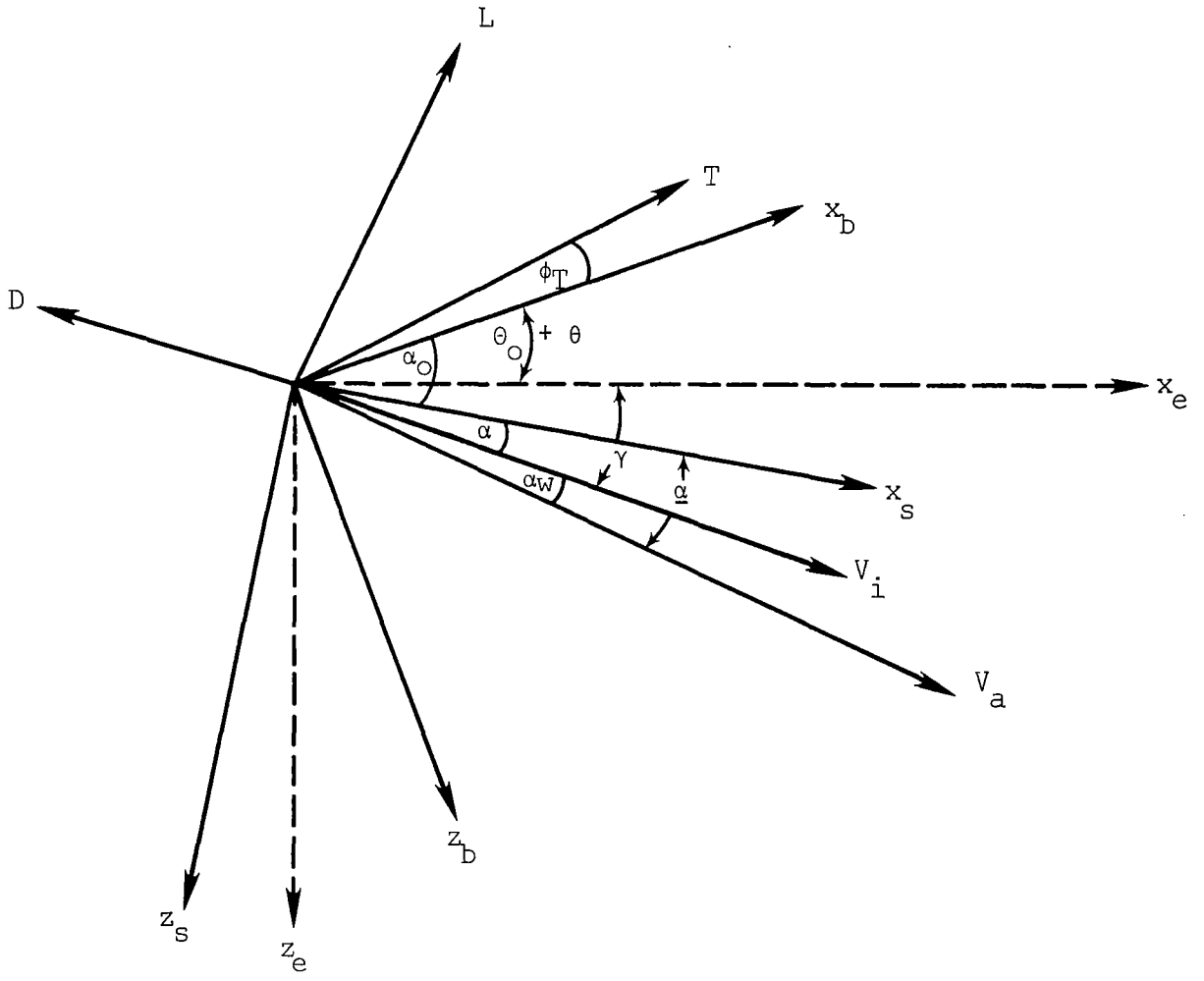

Figure 2 Definition of coordinate axes, angles and forces. (θ_o, θ, ϕ_T are measured positive ccw, α_o, α_w, $\underline{\alpha}$, cw)

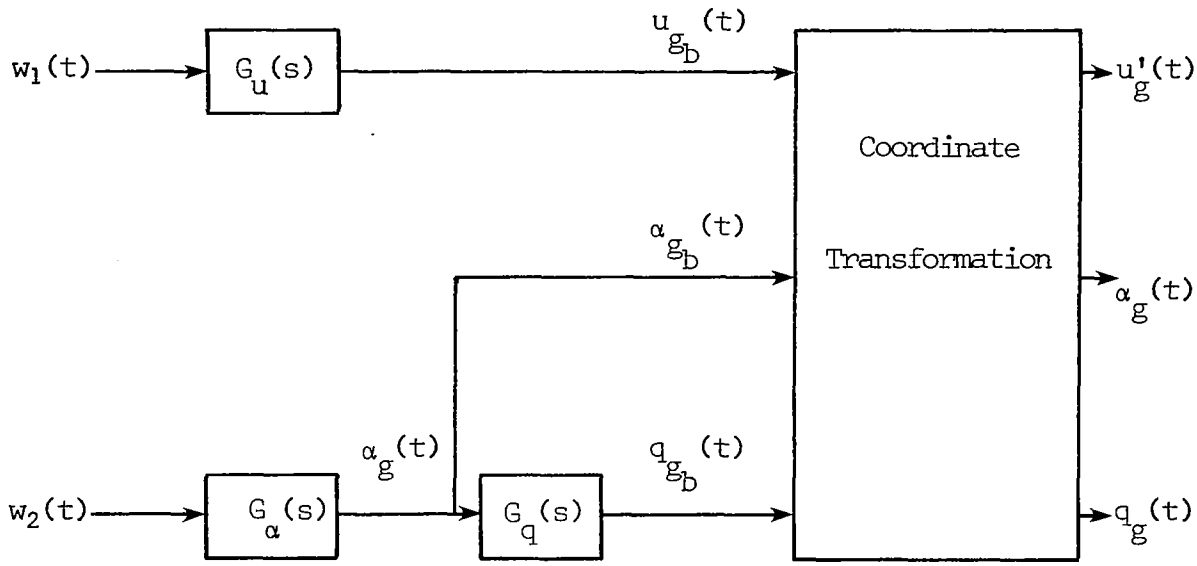

Figure 3 Wind Gust Velocity Model

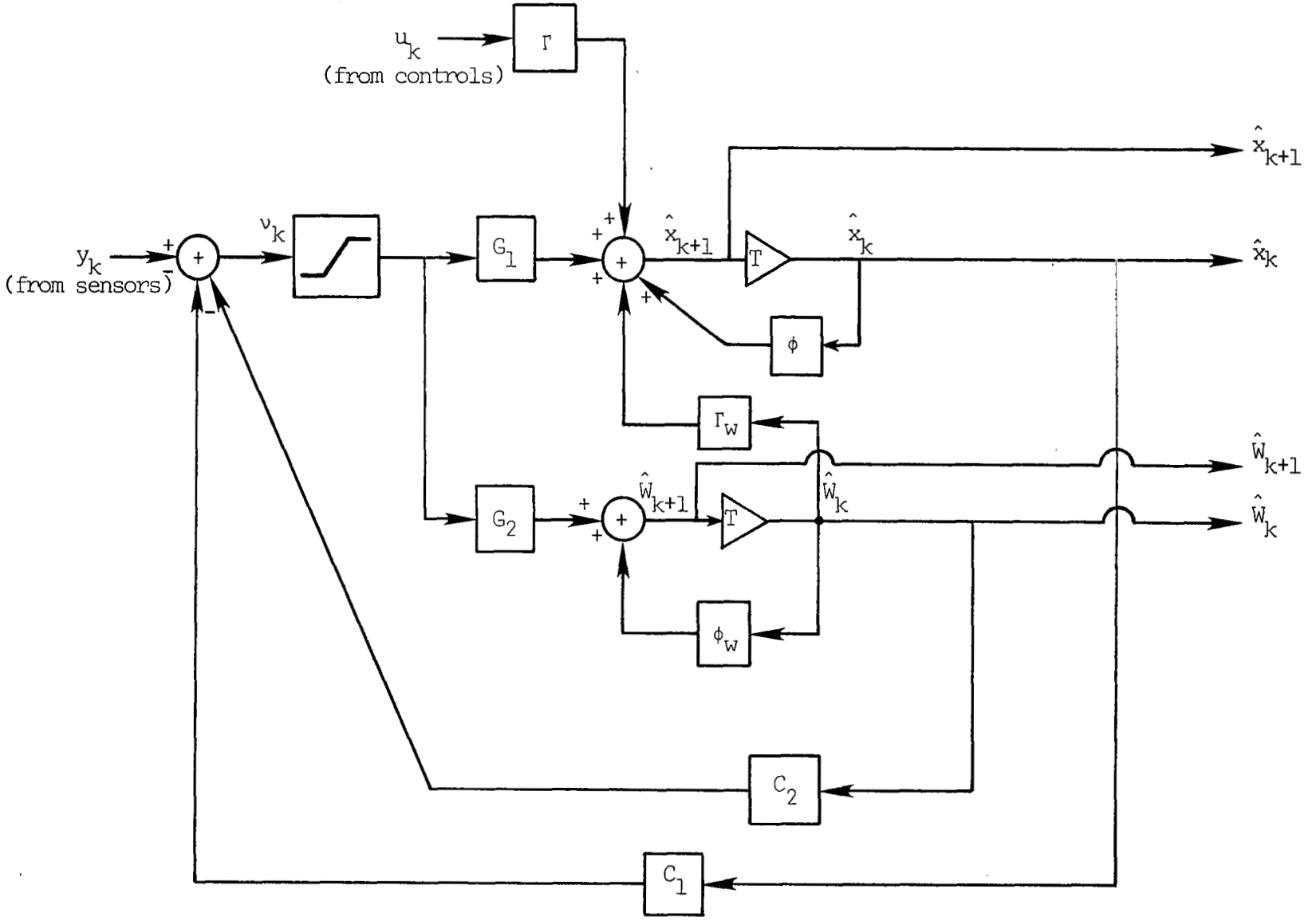

Figure 4 Filter Block Diagram (vectorial form)

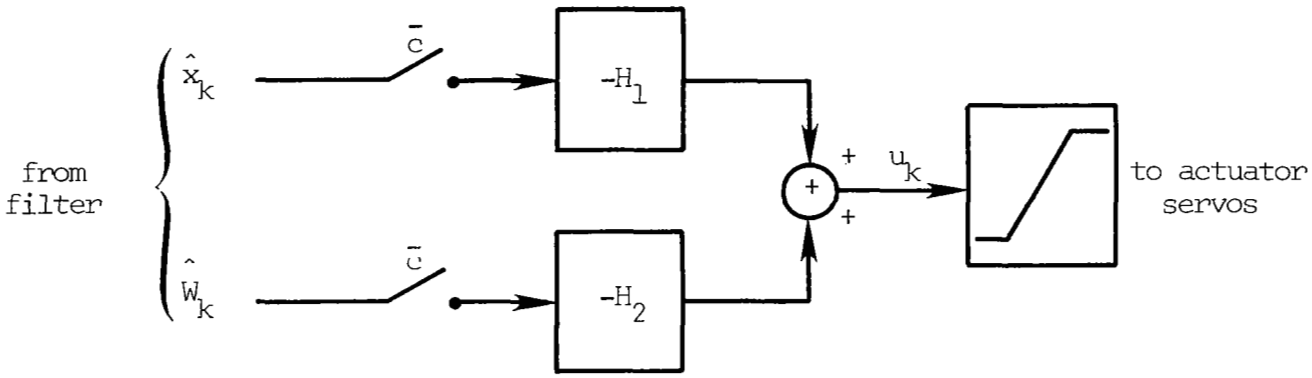

Figure 5 Block Diagram of Control System
($\underline{c}$ is a discrete specifying capture;
$\bar{c}$ means the control system is not
in the glideslope capture mode)

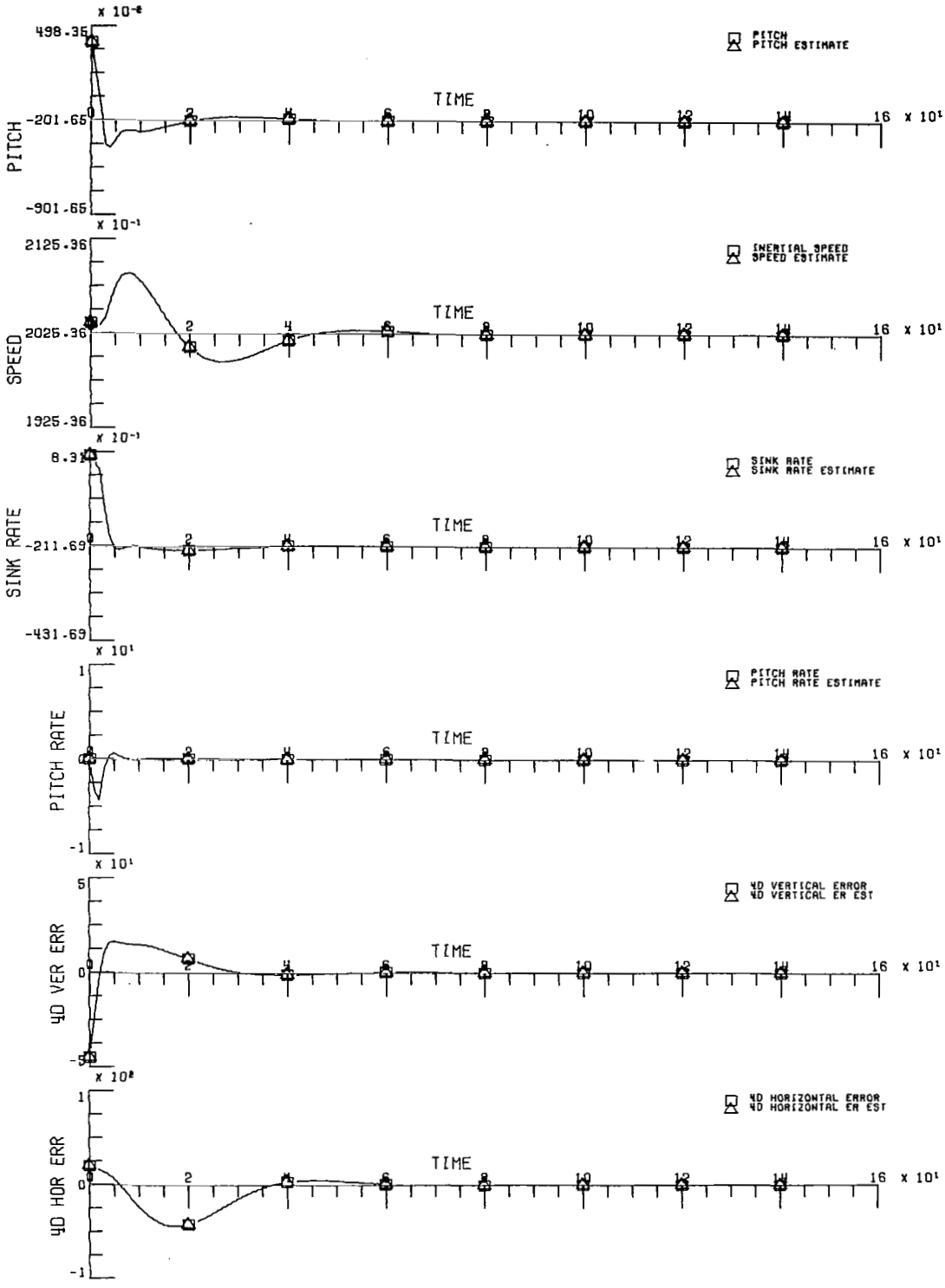

Figure 6a Glideslope Capture and Glideslope Tracking Simulation: No Measurement Noise, No Winds

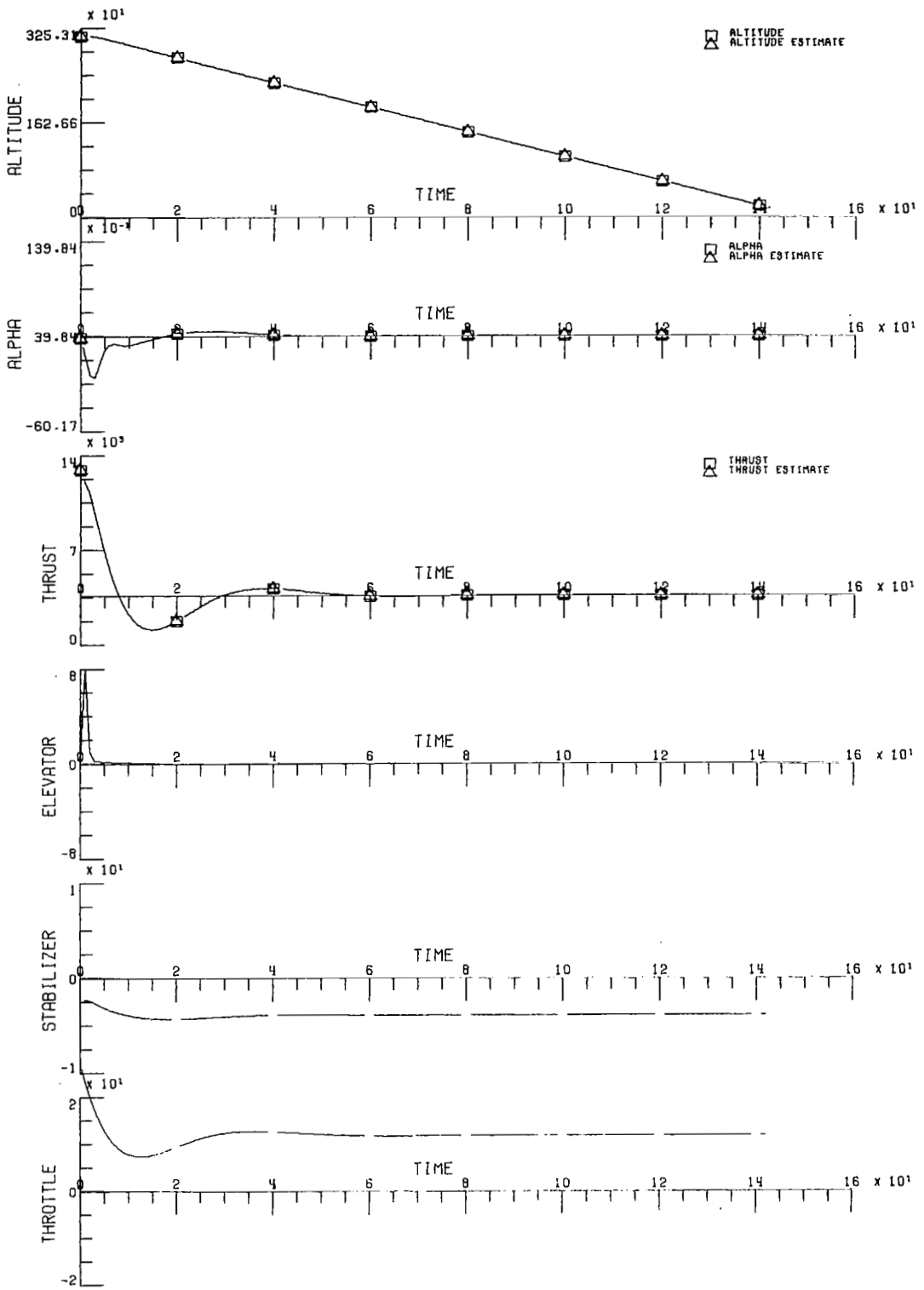
ALTITUDE
x 10¹
325.31
162.66
00
TIME
2
4
6
8
10
12
16 x 10¹
ALTITUDE
ALTITUDE ESTIMATE
ALPHA
x 10⁻¹
139.84
39.84
-60.17
ALPHA ESTIMATE
THRUST
x 10³
14
7
0
THRUST ESTIMATE
ELEVATOR
8
-8
STABILIZER
x 10¹
1
-1
THROTTLE
2
-2

Figure 6b

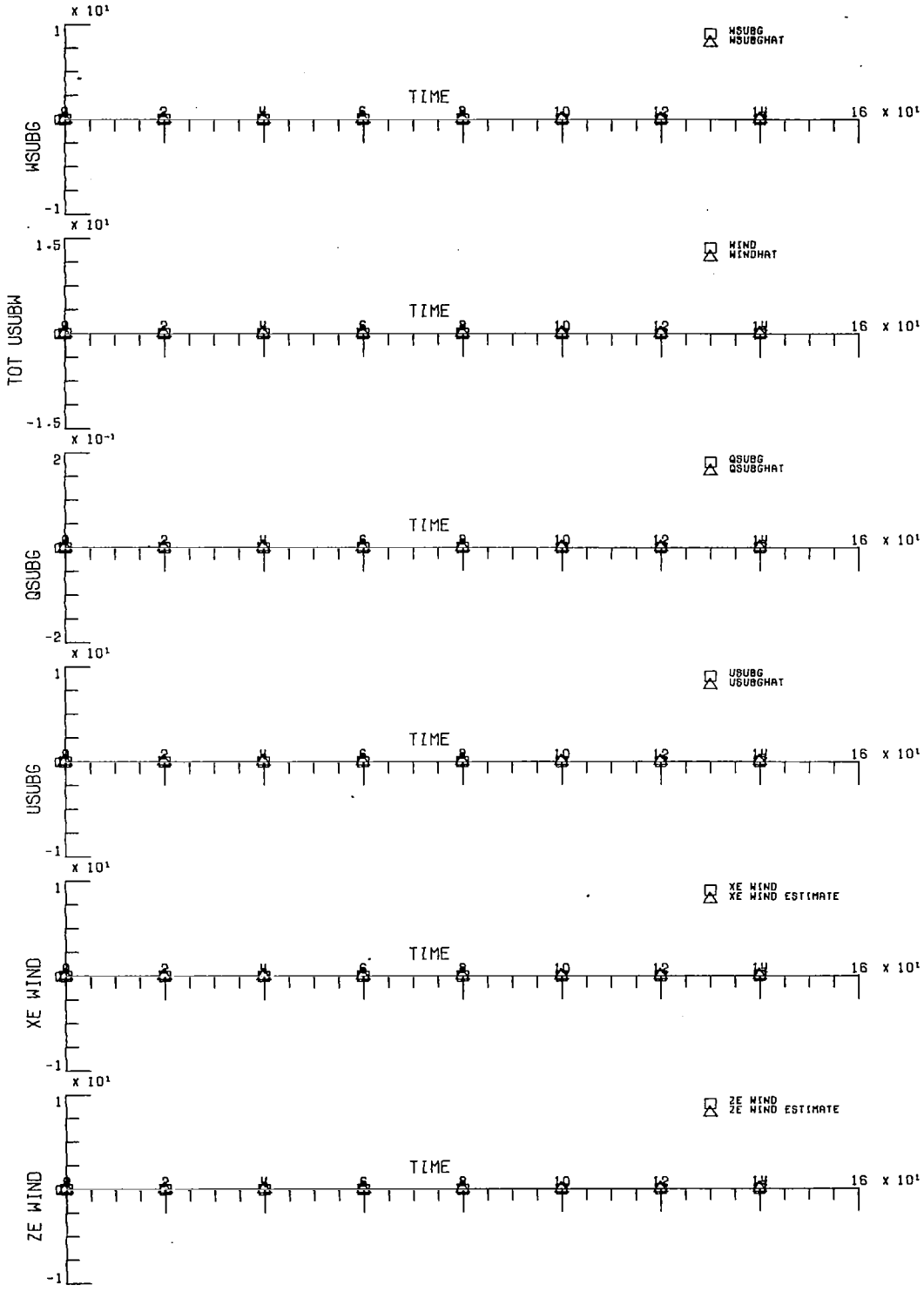
WSUBG
WSUBGHAT
TIME
x 10¹
TOT USUBW
WIND
WINDHAT
QSUBG
QSUBGHAT
USUBG
USUBGHAT
XE WIND
XE WIND ESTIMATE
ZE WIND
ZE WIND ESTIMATE

Figure 6c

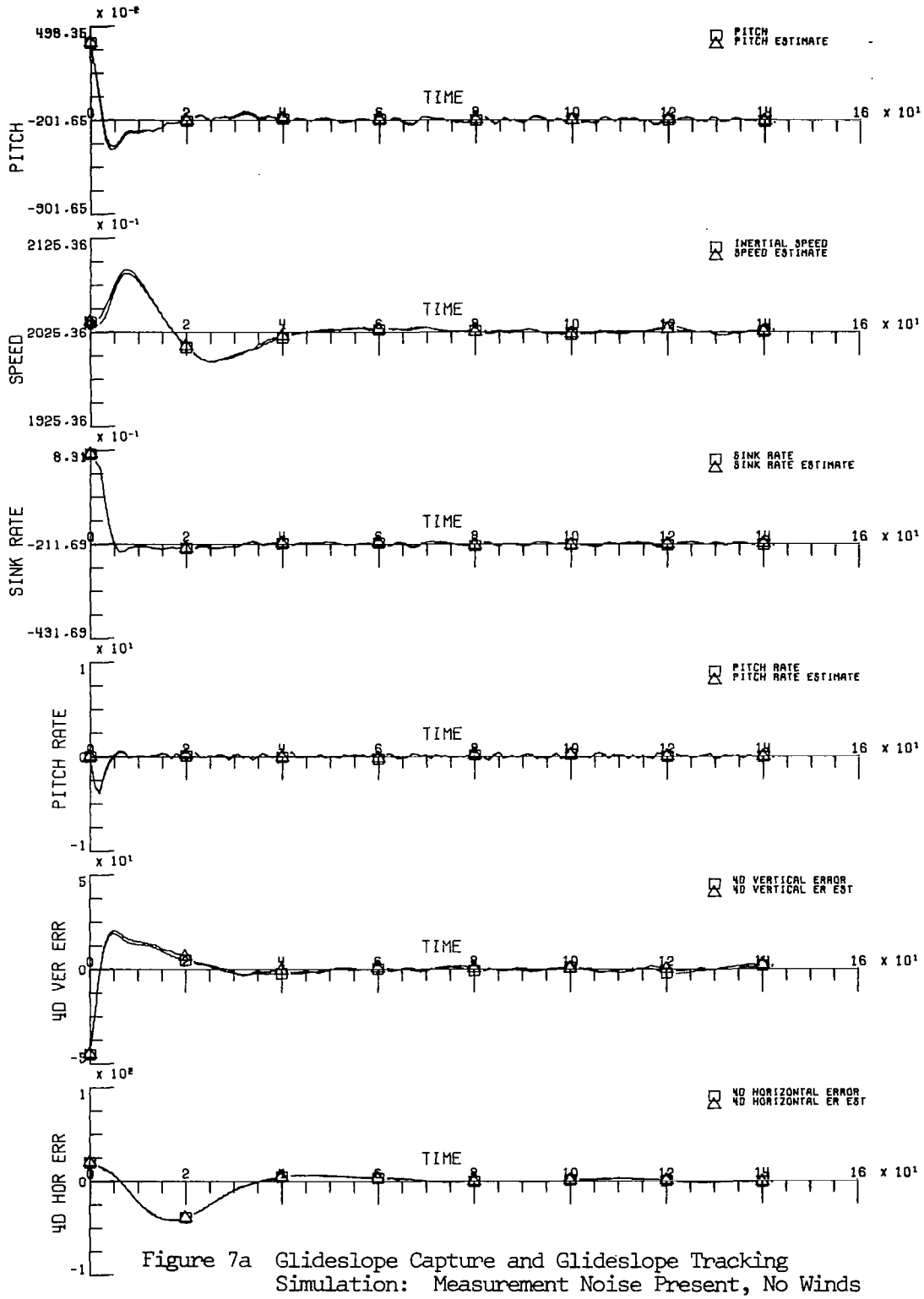

Figure 7a Glideslope Capture and Glideslope Tracking Simulation: Measurement Noise Present, No Winds

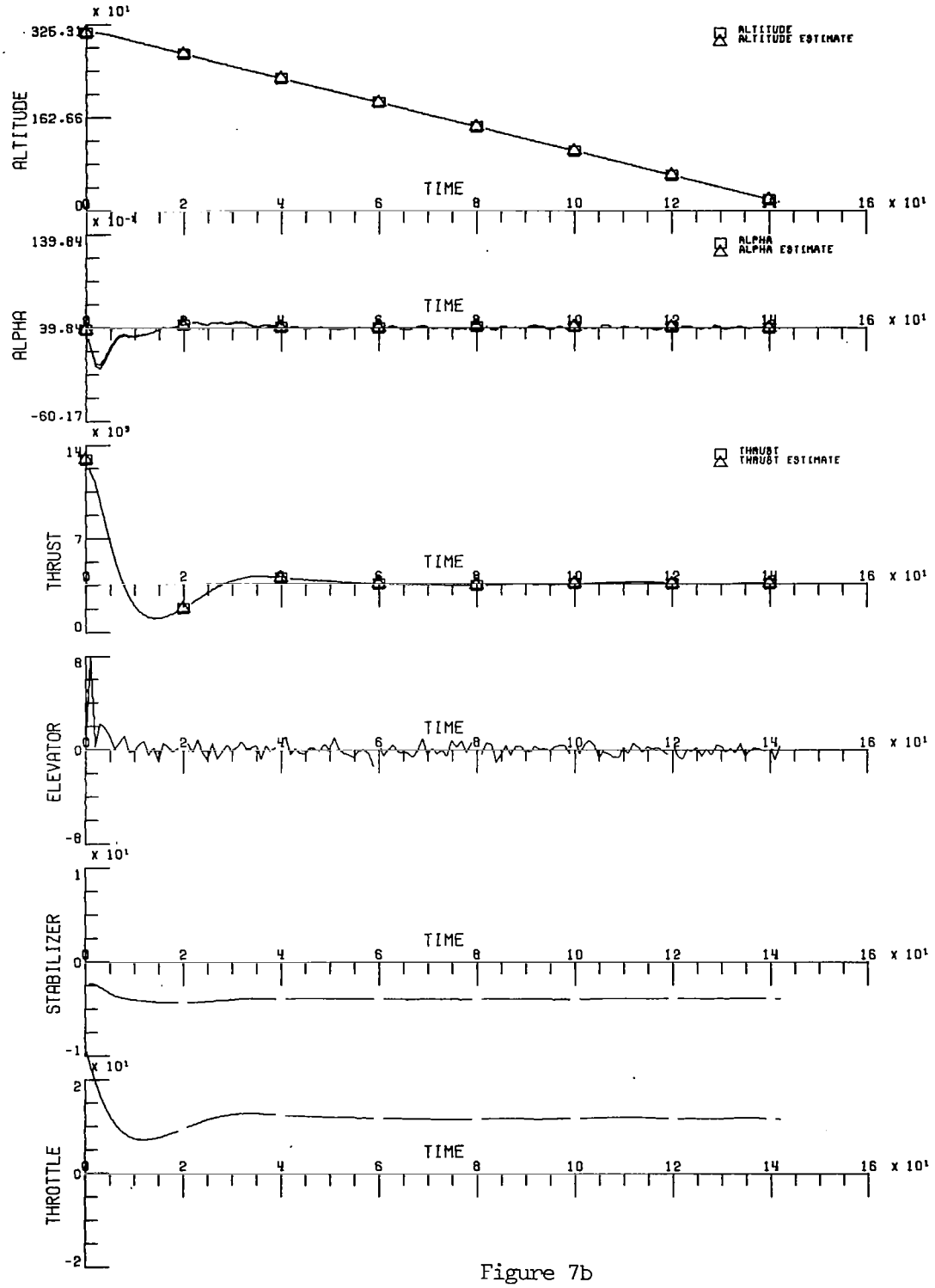
ALTITUDE
ALTITUDE ESTIMATE
ALTITUDE
TIME
ALPHA
ALPHA ESTIMATE
ALPHA
TIME
THRUST
THRUST ESTIMATE
THRUST
TIME
ELEVATOR
TIME
STABILIZER
TIME
THROTTLE
TIME

Figure 7b

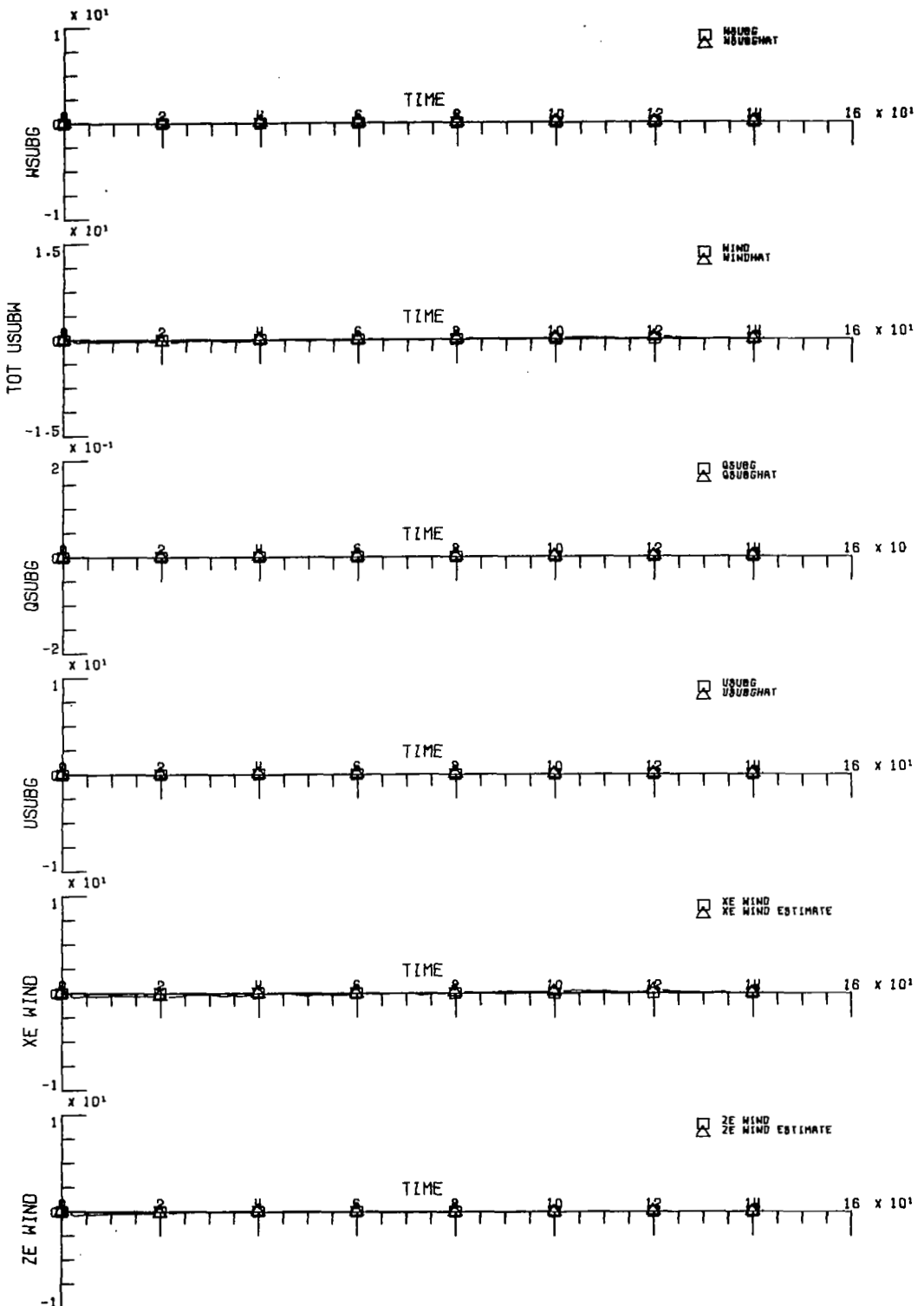
x 10¹
WSUBG
WSUBGHAT
TIME
16 x 10¹
x 10¹
TOT USUBW
WIND
WINDHAT
TIME
16 x 10¹
x 10⁻¹
QSUBG
QSUBGHAT
TIME
16 x 10
x 10¹
USUBG
USUBGHAT
TIME
16 x 10¹
x 10¹
XE WIND
XE WIND ESTIMATE
TIME
16 x 10¹
x 10¹
ZE WIND
ZE WIND ESTIMATE
TIME
16 x 10¹

Figure 7c

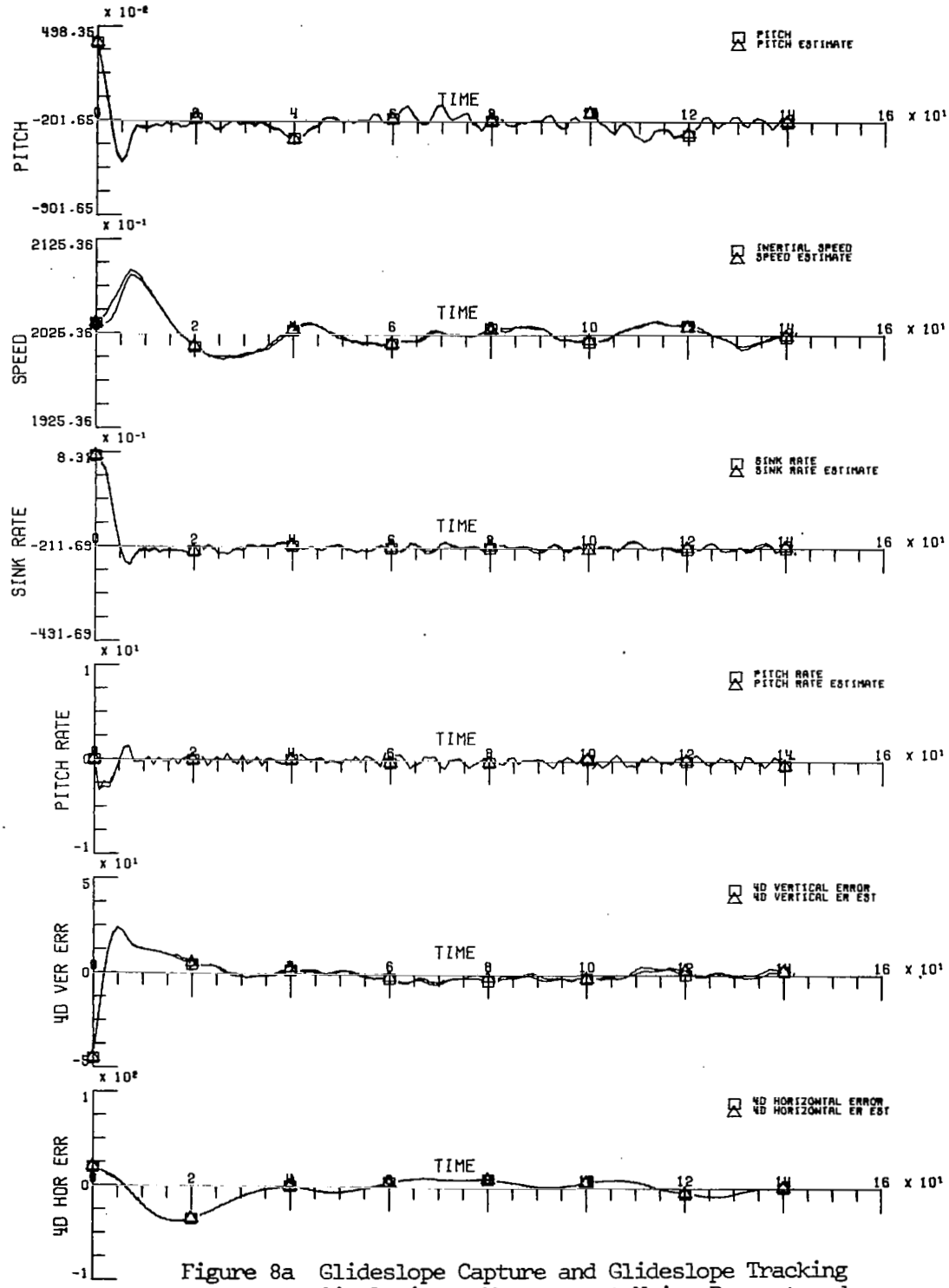

Figure 8a Glideslope Capture and Glideslope Tracking Simulation: Measurement Noise Present and Average Wind Gust (σ_u = 2 ft/sec., σ_ω = 1 ft/sec.)

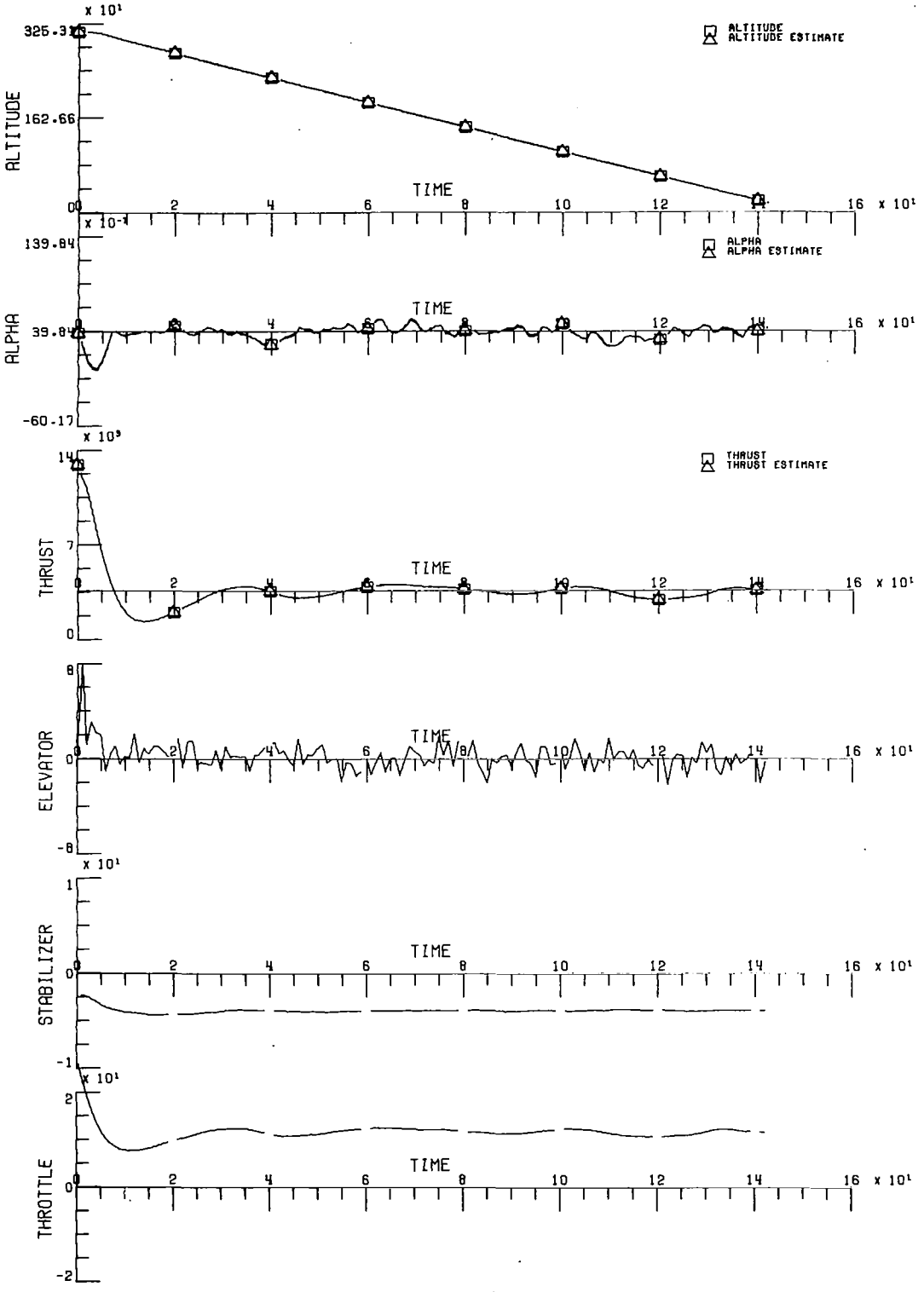
ALTITUDE
ALTITUDE ESTIMATE
ALPHA
ALPHA ESTIMATE
THRUST
THRUST ESTIMATE
TIME
ALTITUDE
ALPHA
THRUST
ELEVATOR
STABILIZER
THROTTLE

Figure 8b

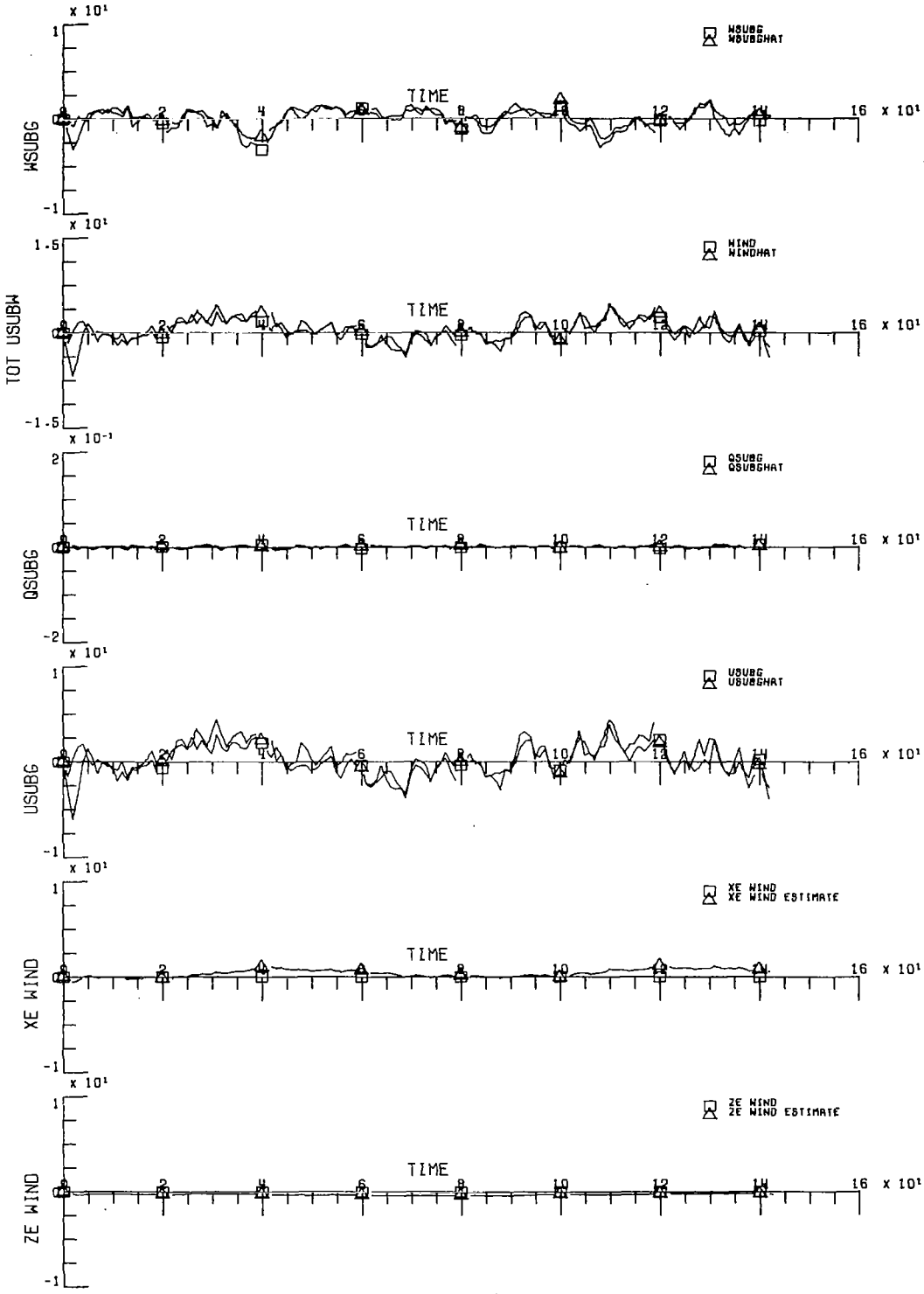
WSUBG
WSUBGHAT
TIME
WSUBG
x 10¹
WIND
WINDHAT
TOT USUBW
QSUBG
QSUBGHAT
USUBG
USUBGHAT
XE WIND
XE WIND ESTIMATE
ZE WIND
ZE WIND ESTIMATE
16 x 10¹

Figure 8c

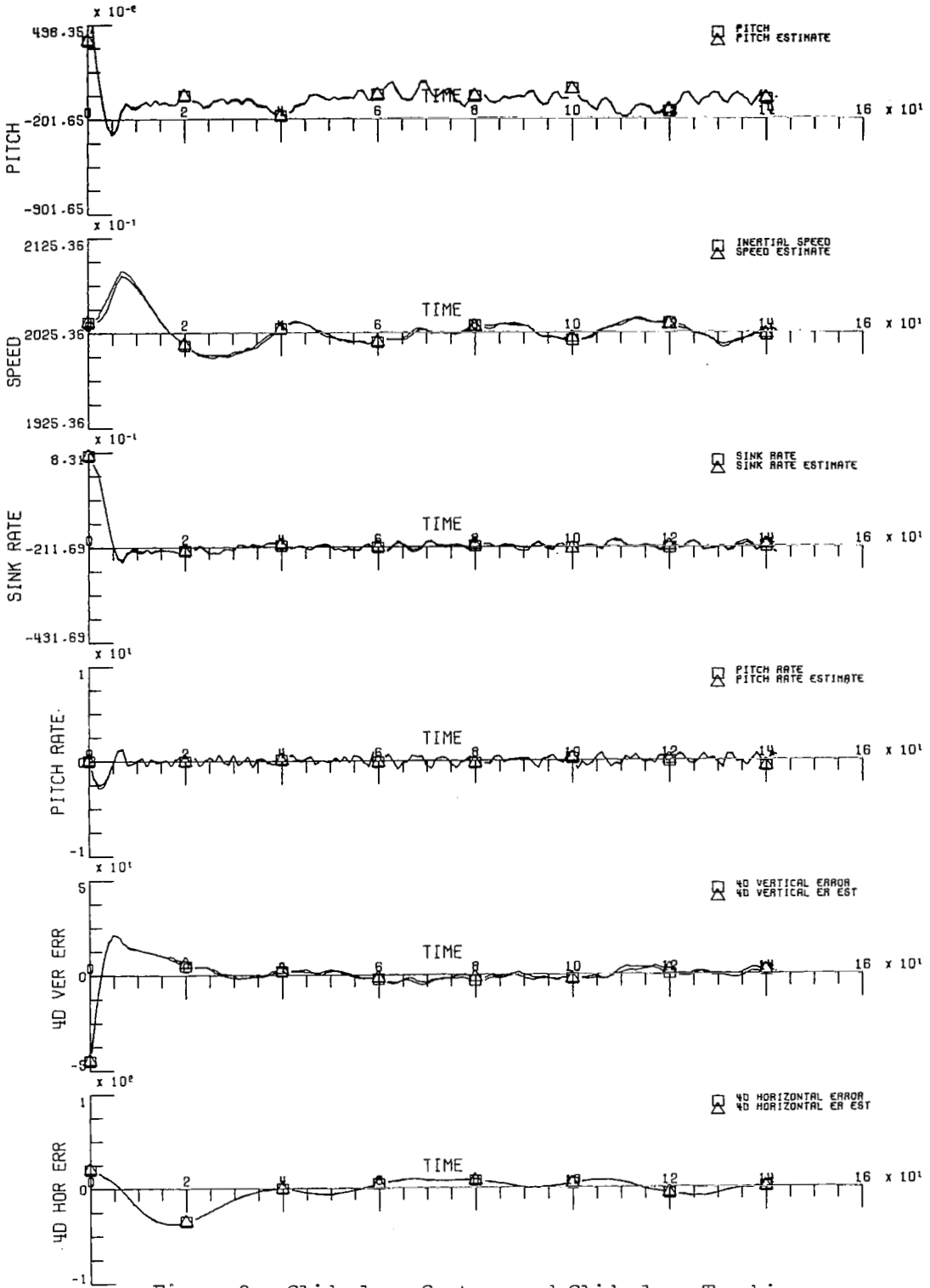

Figure 9a Glideslope Capture and Glideslope Tracking Simulation: Measurement Noise Present, Average Wind Gusts (σ_u = 2 ft/sec., σ_ω = 1 ft/sec.), Tail Wind of 8 ft.sec.

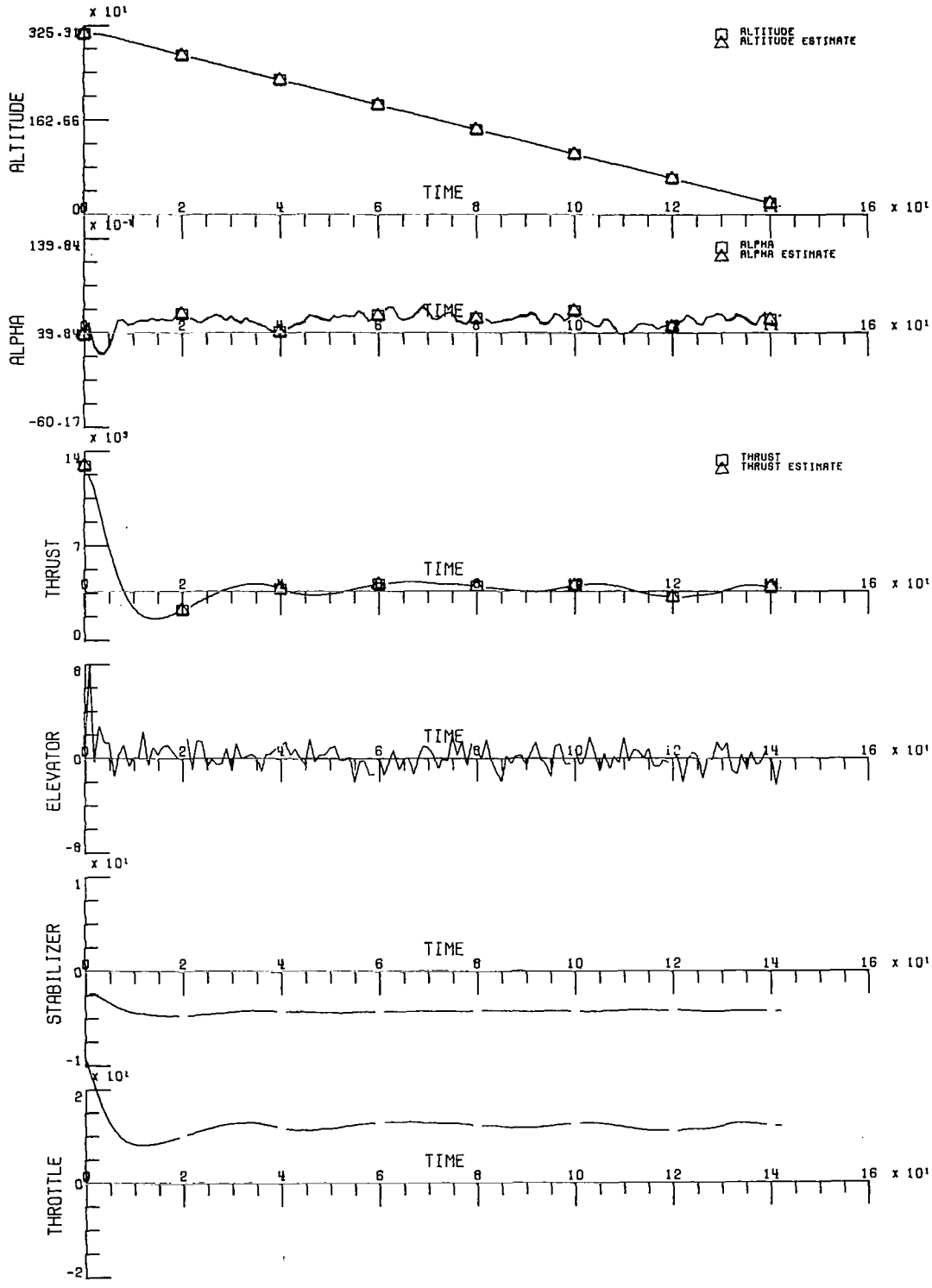
ALTITUDE
ALTITUDE ESTIMATE
ALTITUDE
TIME
ALPHA
ALPHA ESTIMATE
ALPHA
TIME
THRUST
THRUST ESTIMATE
THRUST
TIME
ELEVATOR
TIME
STABILIZER
TIME
THROTTLE
TIME

Figure 9b

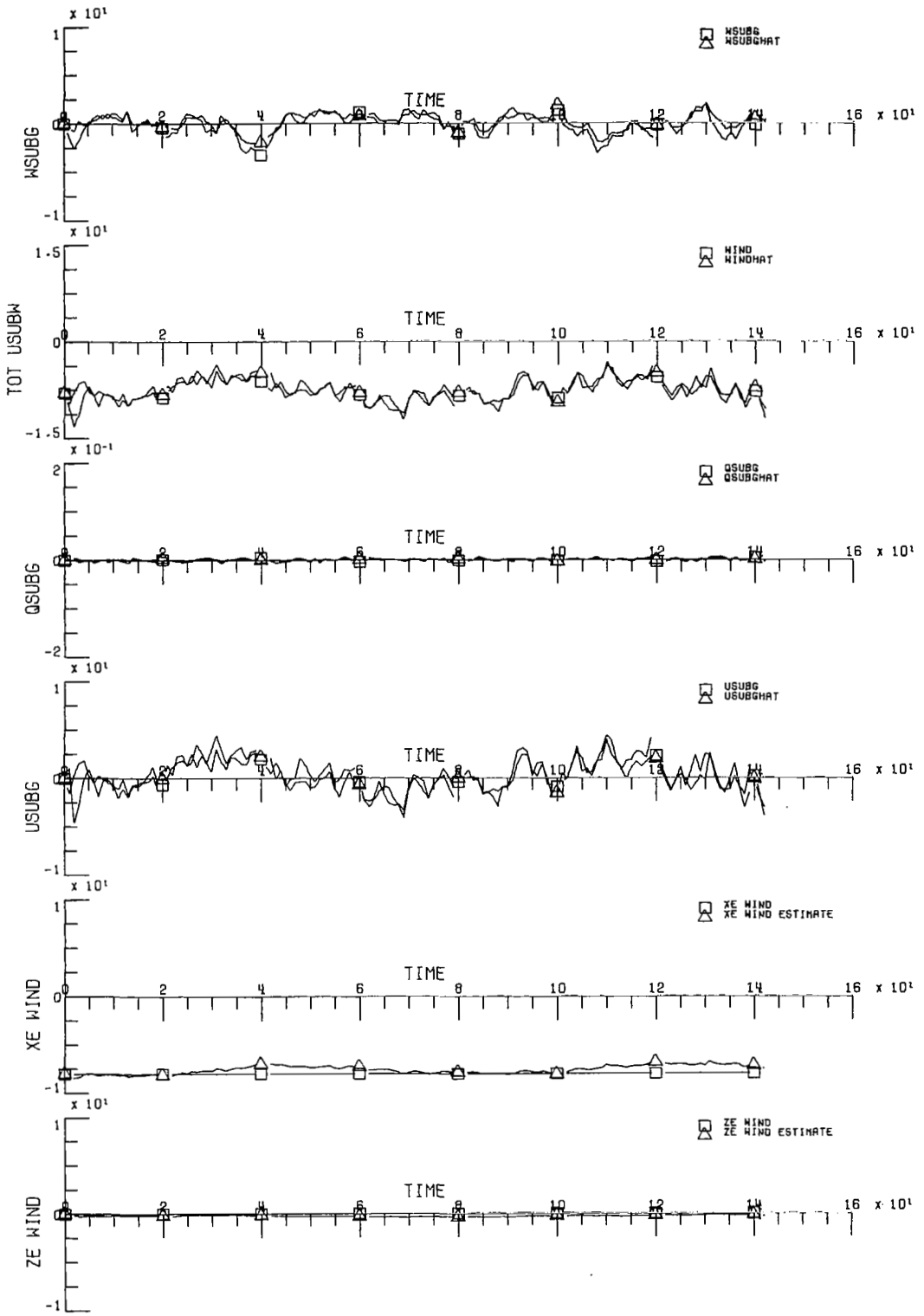
WSUBG
WSUBGHAT
TIME
WSUBG
x 10¹
WIND
WINDHAT
TOT USUBW
QSUBG
QSUBGHAT
x 10⁻¹
USUBG
USUBGHAT
XE WIND
XE WIND ESTIMATE
ZE WIND
ZE WIND ESTIMATE

Figure 9c

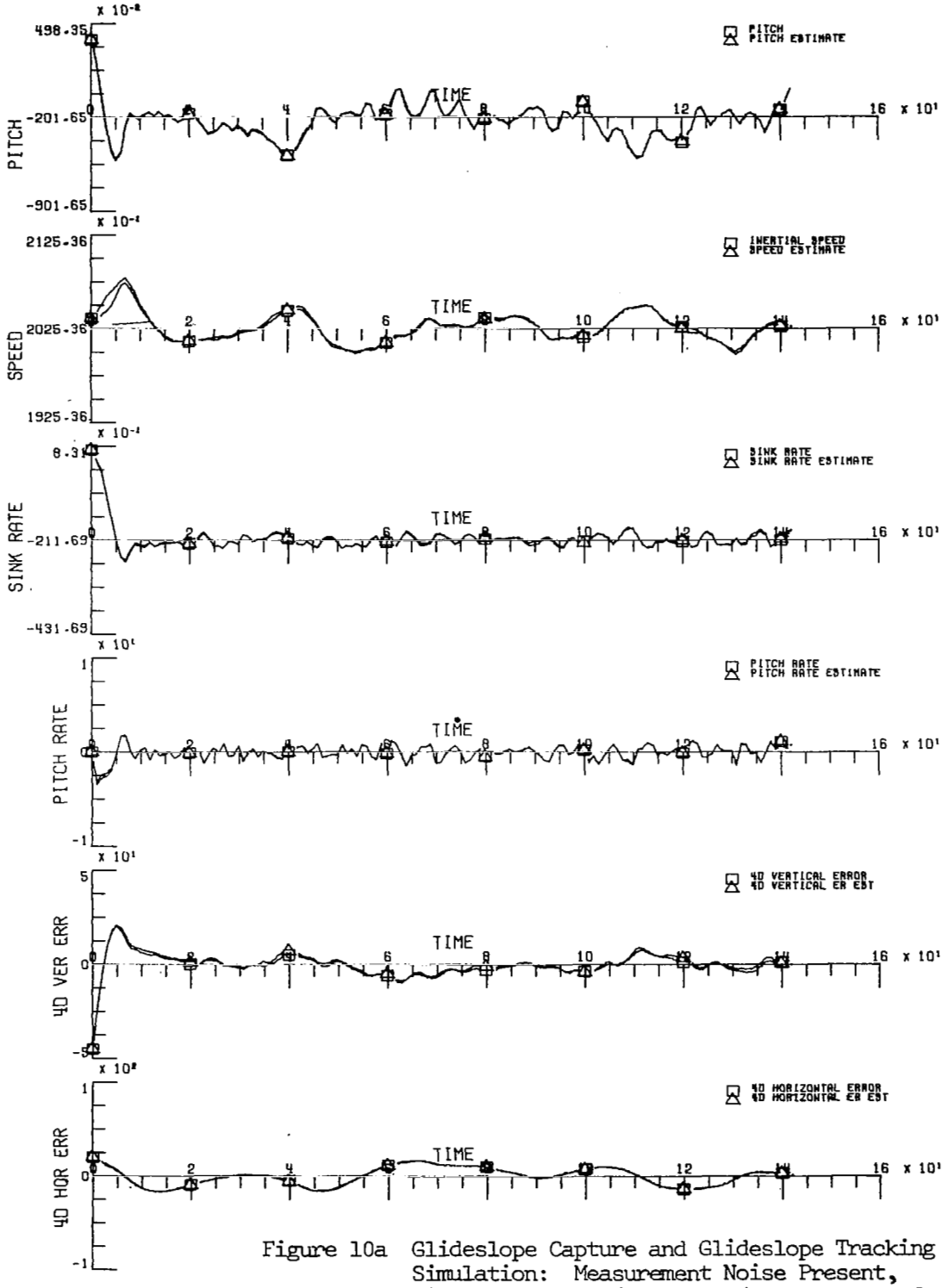

Figure 10a Glideslope Capture and Glideslope Tracking Simulation: Measurement Noise Present, High Wind Gusts (σ_u = 4 ft/sec., σ_ω = 2 ft/sec.)

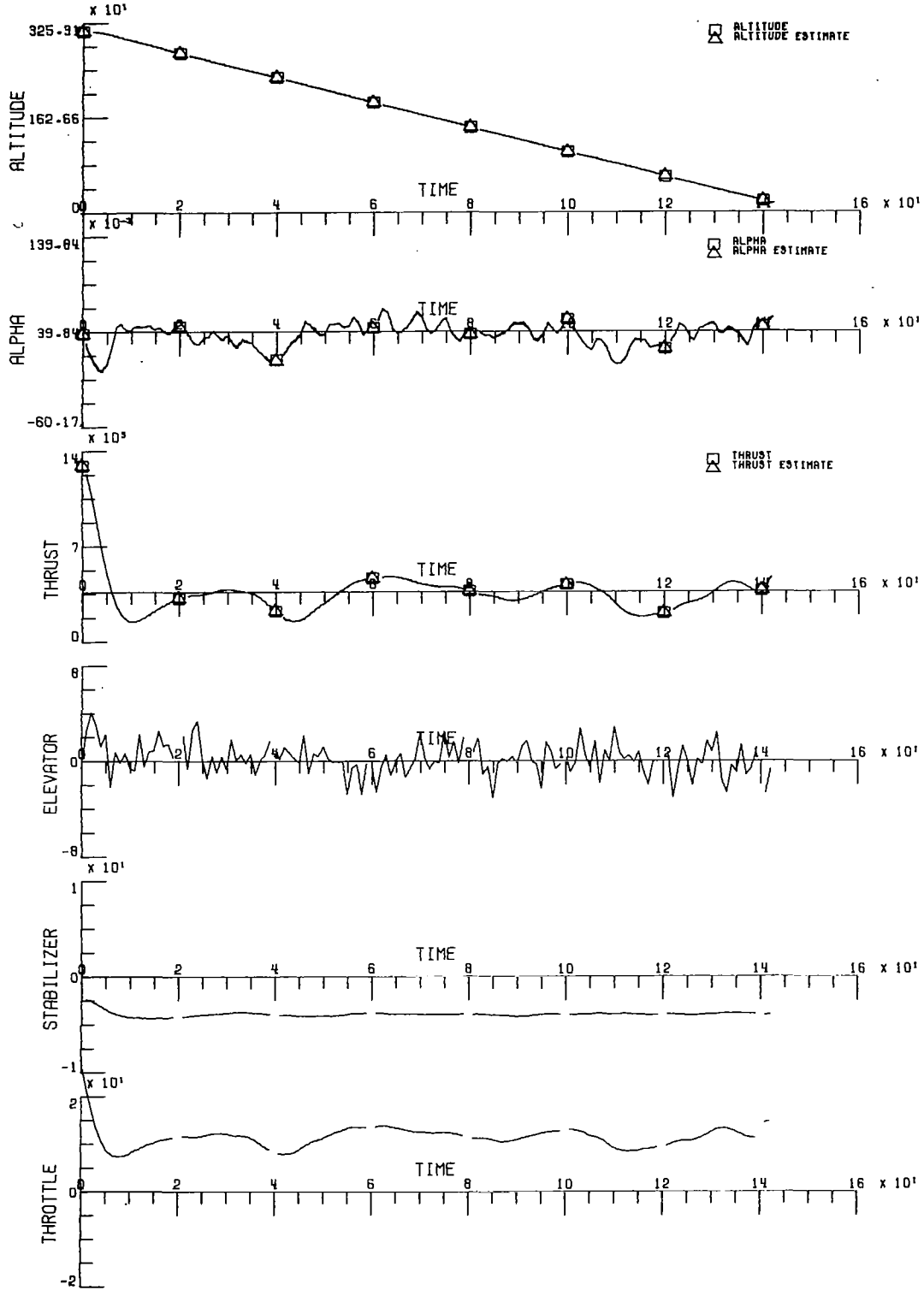
ALTITUDE
ALTITUDE ESTIMATE
ALTITUDE
TIME
ALPHA
ALPHA ESTIMATE
ALPHA
TIME
THRUST
THRUST ESTIMATE
THRUST
TIME
ELEVATOR
TIME
STABILIZER
TIME
THROTTLE
TIME

Figure 10b

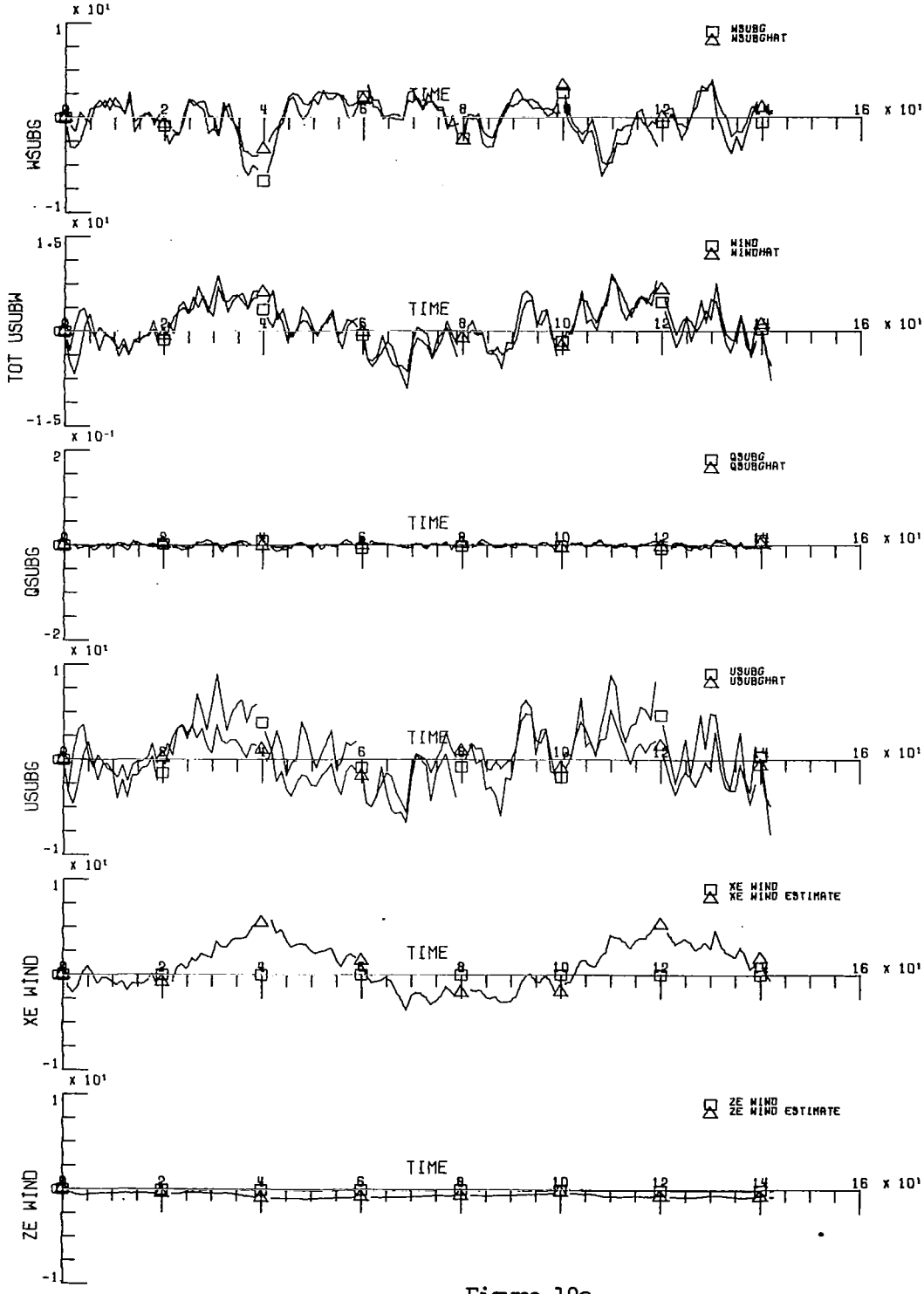
WSUBG
WSUBGHAT
TIME
TOT USUBW
WIND
WINDHAT
QSUBG
QSUBGHAT
USUBG
USUBGHAT
XE WIND
XE WIND ESTIMATE
ZE WIND
ZE WIND ESTIMATE
x 10¹
x 10⁻¹

Figure 10c

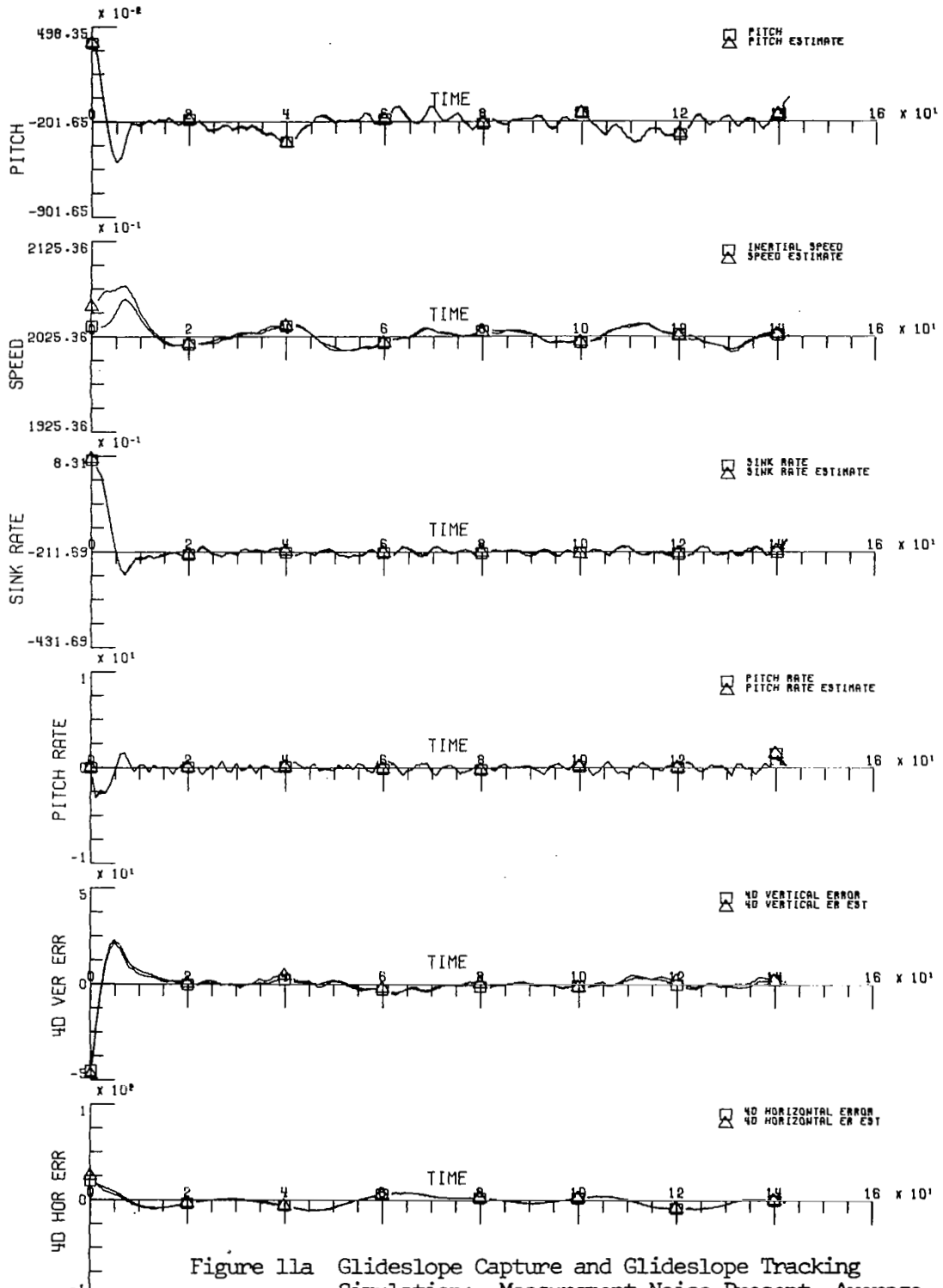

Figure 11a Glideslope Capture and Glideslope Tracking Simulation: Measurement Noise Present, Average Wind Gusts (σ_u = 2 ft/sec., σ_ω = 1 ft/sec.) and Initial Estimate Errors

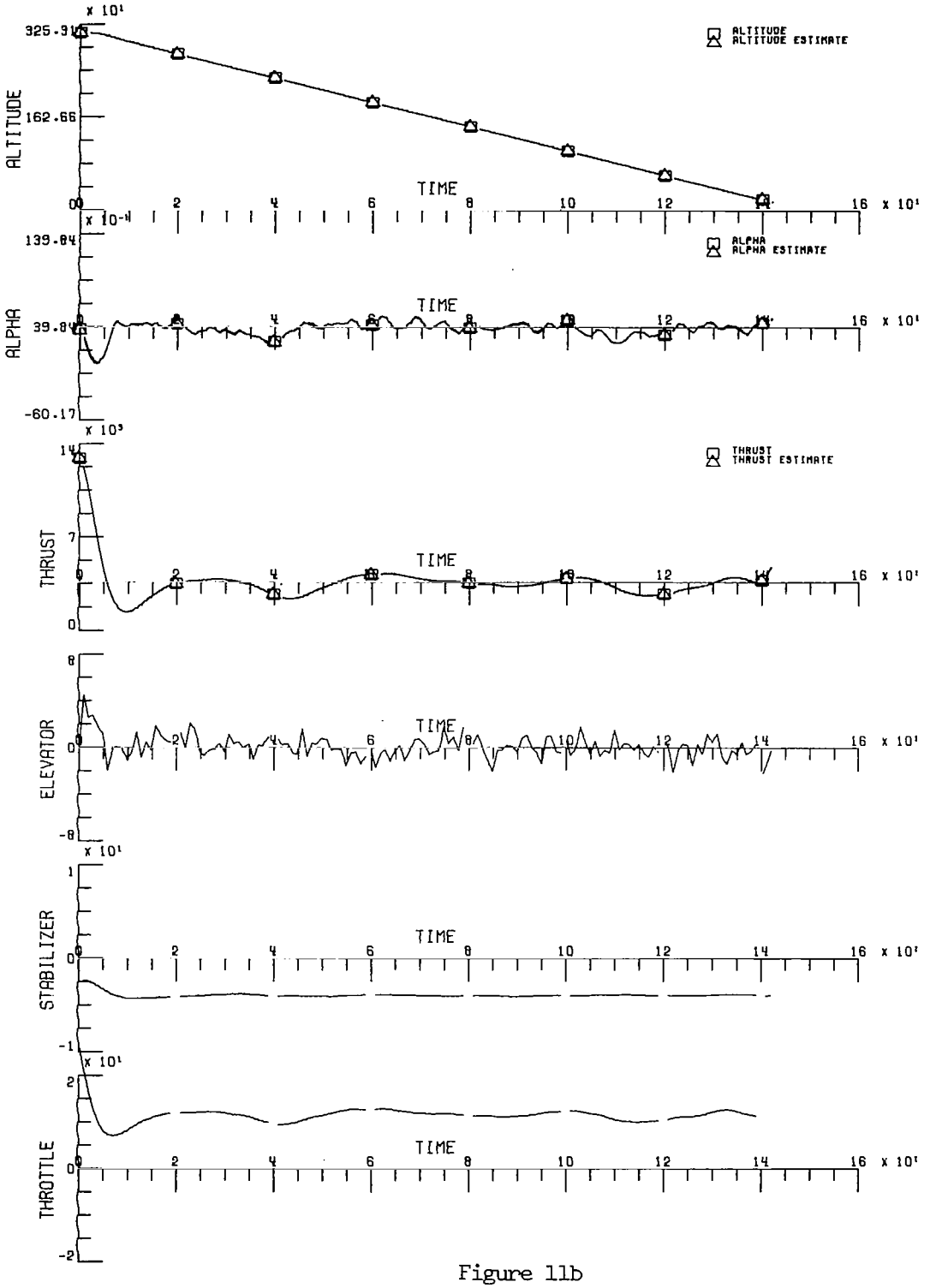
ALTITUDE
ALTITUDE ESTIMATE
ALPHA
ALPHA ESTIMATE
THRUST
THRUST ESTIMATE
TIME

Figure 11b

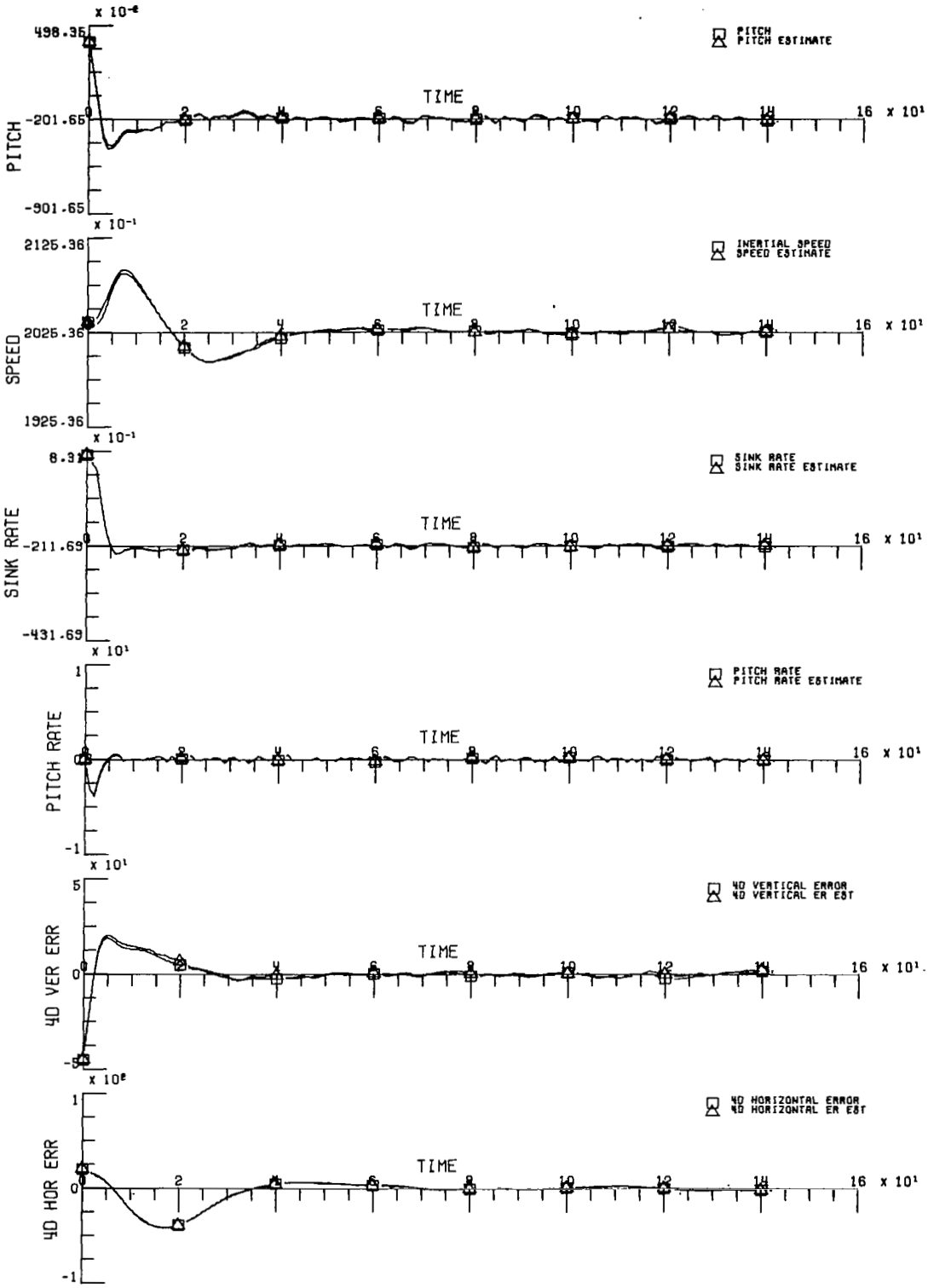
x 10⁻⁶
498.36
-201.65
-901.65
PITCH
PITCH
PITCH ESTIMATE
TIME
0
2
4
6
8
10
12
14
16 x 10¹
x 10⁻¹
2125.36
2025.36
1925.36
SPEED
INERTIAL SPEED
SPEED ESTIMATE
x 10⁻¹
8.3
-211.69
-431.69
SINK RATE
SINK RATE
SINK RATE ESTIMATE
x 10¹
1
0
-1
PITCH RATE
PITCH RATE
PITCH RATE ESTIMATE
x 10¹
5
0
-5
4D VER ERR
4D VERTICAL ERROR
4D VERTICAL ER EST
x 10⁰
1
0
-1
4D HOR ERR
4D HORIZONTAL ERROR
4D HORIZONTAL ER EST

Figure 11c

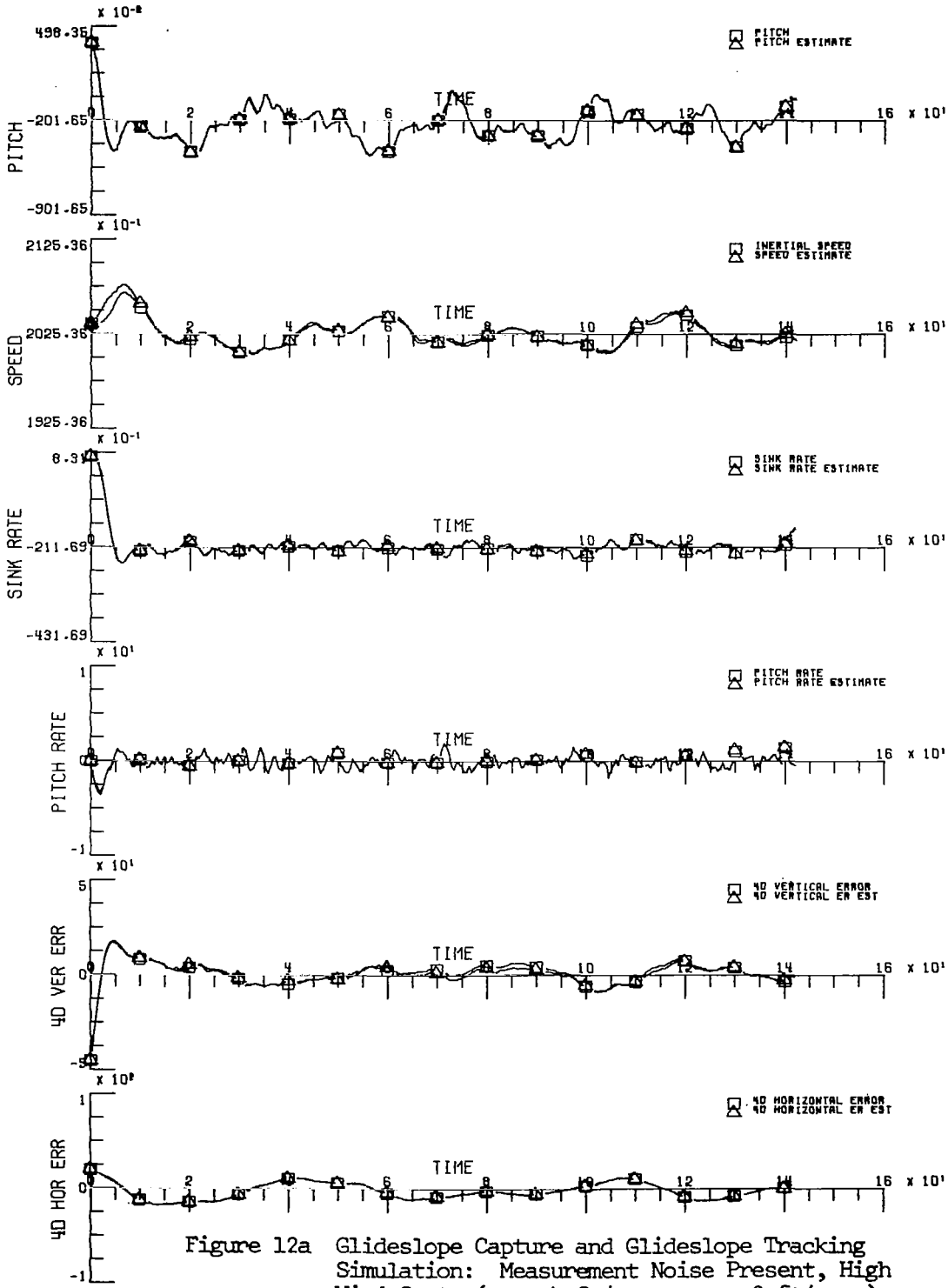

Figure 12a Glideslope Capture and Glideslope Tracking Simulation: Measurement Noise Present, High Wind Gusts (σ_u = 4 ft/sec., σ_ω = 2 ft/sec.), Sampling Rate 10/sec.

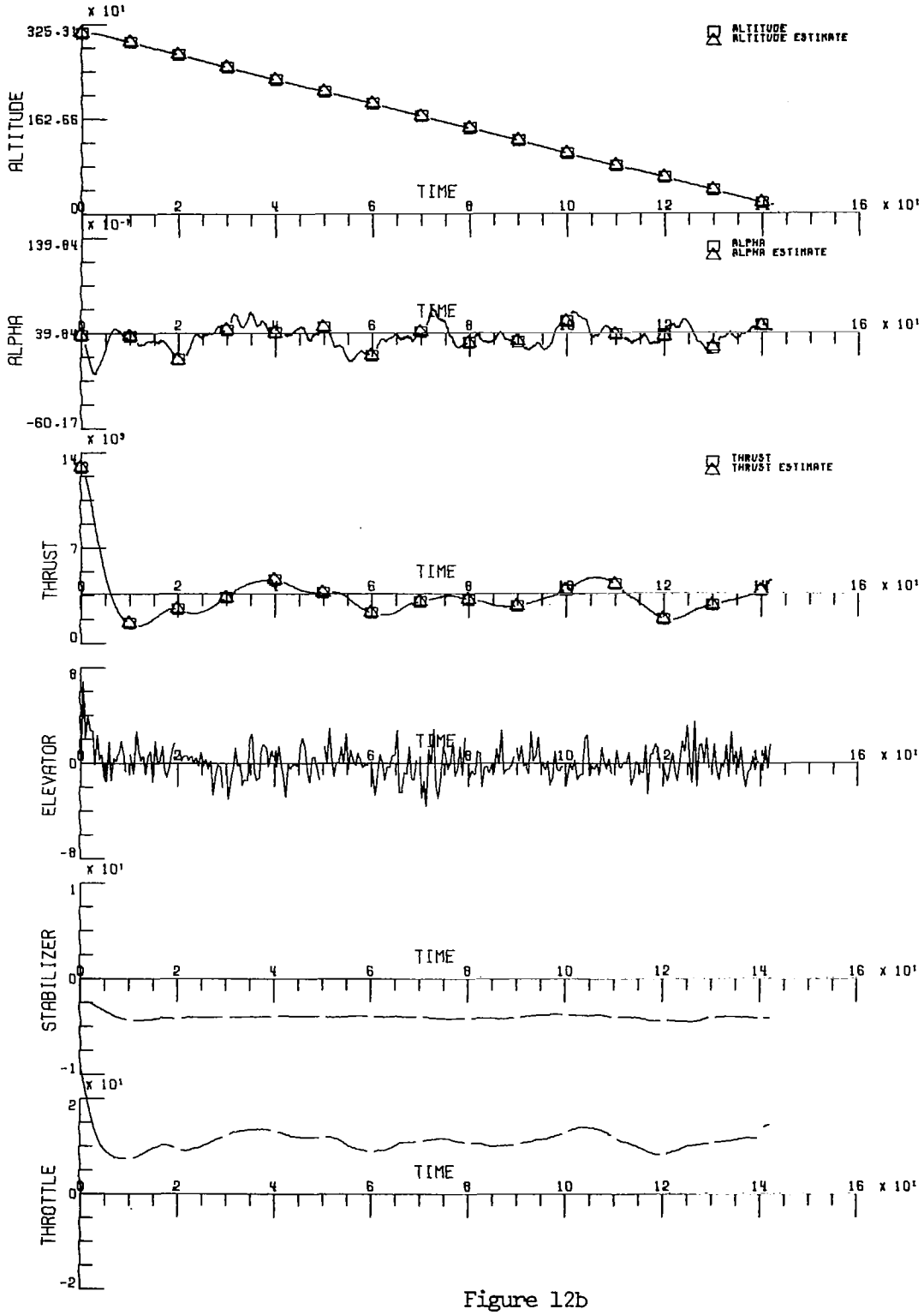
ALTITUDE
ALTITUDE ESTIMATE
ALTITUDE
TIME
ALPHA
ALPHA ESTIMATE
ALPHA
TIME
THRUST
THRUST ESTIMATE
THRUST
TIME
ELEVATOR
TIME
STABILIZER
TIME
THROTTLE
TIME

Figure 12b

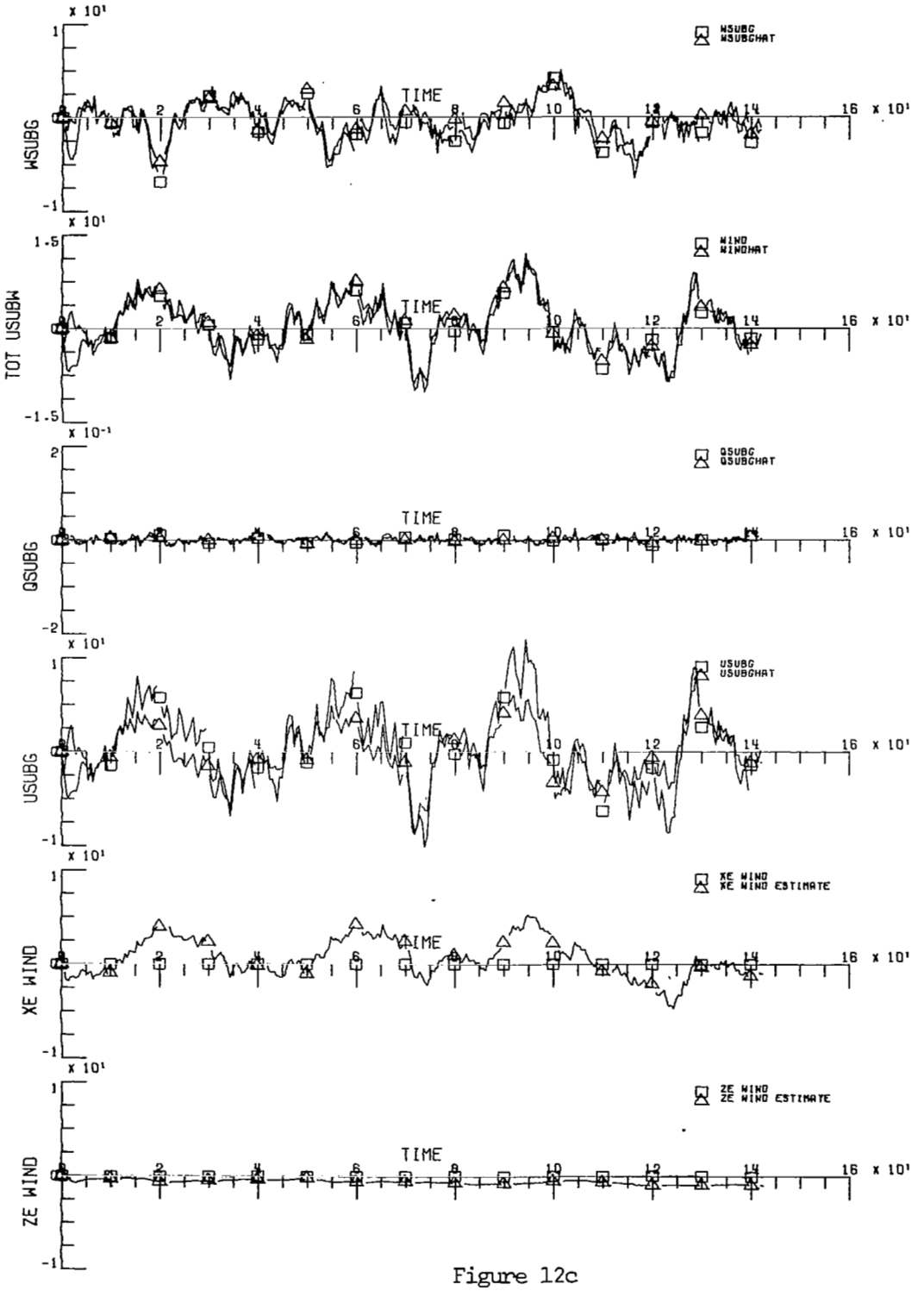
WSUBG
WSUBGHAT
TOT USUBW
WIND
WINDHAT
QSUBG
QSUBGHAT
USUBG
USUBGHAT
XE WIND
XE WIND ESTIMATE
ZE WIND
ZE WIND ESTIMATE
TIME
x 10¹
x 10⁰
x 10⁻¹

Figure 12c

Table 1 Standard Deviation Values for the Simulation of Sensor Noises

Variable	Standard Deviation	Type
Y_1	.15°	additive
Y_2	.10°/sec	additive
Y_3	1 ft.	additive
Y_4	.031°	additive
Y_5	25 ft.	additive
Y_6	5 %	multiplicative
Y_7	.005 g	additive
Y_8	2 %	multiplicative
Y_9	.005 g	additive

References

1. Reeder, J. P., R. T. Taylor and T. M. Walsh, "New designs and operating techniques for improved terminal area compatability," SAE, Air transportation meeting, Dallas, Texas, April 30, 1974.

2. Anon., "A new guidance system for approach and landing," Vol. 2, Radio Technical Commission for Aeronautics, 1717 H Street, N. W., Washington, D. C., Document DO-148, Dec. 18, 1970.

3. Cicolani, L. S., "Position determination accuracy from the Microwave Landing System," NASA TN D-7116, NASA Ames Research Center, Calif.

4. Etkin, B., Dynamics of Atmospheric Flight, John Wiley & Sons, Inc., New York, 1972.

5. Roskam, J., Flight dynamics of rigid and elastic airplanes, Roskam Aviation and Engineering Corp., 519 Boulder, Lawrence, Kansas, 1972.

6. McRuer, D., I. Ashkenas, D. Graham, Aircraft Dynamics and Automatic Control, Princeton University Press, Princeton, New Jersey, 1973.

7. Sage, A. P. and J. L. Melsa, Estimation Theory with Applications to Communications and Control, McGraw-Hill, New York, 1971.

8. Loève, M., Probability theory, D. Van Nostrand Co., Princeton, New Jersey, 1955.

9. Chalk, C. R., T. P. Neal, T. M. Harris and E. F. Prichard, "Background information and user guide for MIL-F-8785B(ASG), 'Military Specification - flying qualities of piloted airplanes,'" Air Force Flight Dynamics REport AFFDL-TR-69-72, Aug. 1969.

10. Barr, N. M., D. Gangsaas and D. R. Schaeffer, "Wind models for flight simulator certification of landing and approach guidance and control systems," FAA SRDS, Report No. RD-74-206, Dec. 1974.

11. Bode, H. W. and C. E. Shannon, "A simplified derivation of linear least-squares smoothing and prediction theory," Proc. IRE, Vol. 38, pp. 417-425, April 1950.

12. Anderson, B. D. O., J. B. Moore and S. B. Loo, "Spectral factorization of time-varying covariance functions," IEEE Trans. on Info. Theo., Vol. IT-15, pp. 550-557, Sept. 1959.

13. Halyo, N. and G. A. McAlpine, "On the spectral factorization of non-stationary vector random processes," IEEE Trans. on Automatic Control, Vol. AC-19, No. 6, Dec. 1974.

14. Ogata, K., State space analysis of control systems, Prentice Hall, New Jersey, 1967.

15. Halyo, N. and A. Caglayan, "A separation theorem for the stochastic sampled-data LQG problem," International J. of Control, to be published.

16. Hoffman, W. C., W. M. Hollister and R. W. Simpson, "Functional error analysis and modeling for ATC system concepts evaluation," DOT, TSC-212-72-1, May 1972.

17. Sorensen, J. A., "Analysis of instrumentation error effects on the identification of aircraft parameters," NASA CR-112121, 1972.

18. Montgomery, R. C., "Analytic design of digital flight controllers to realize aircraft flying quality specifications," J. of Aircraft, Vol. 9, No. 7, pp. 456-460, July 1972.

19. Kalman, R. E., "A new approach to linear filtering and prediction problems," Trans. ASME, J. Basic Eng., Vol. 82, pp. 34-35, March 1960.

20. Kailath, T., "An innovations approach to least-squares estimation, part I: linear filtering in additive white noise," IEEE Trans. Auto. Contr., Vol. AC-13, pp. 655-660, Dec. 1968.

21. Kushner, H. J., Introduction to stochastic control, Holt, Rinehart and Winston, New York, 1971.

22. Special issue on linear-quadratic-gaussian problem, IEEE Trans. on Auto. Control, Vol. AC-16, Dec. 1971.

23. Johnson, C. D., "Optimal control of the linear regulator with constant disturbances," IEEE Trans. on Auto Control, Vol. AC-13, pp. 416-421, 1968.

24. _____, "Accommodation of external disturbance in linear regulator and servomechanism problems," IEEE Trans. on Auto. Control, Vol. AC-16, pp. 635-644, 1971.

25. _____, "Accommodation of disturbances in optimal control problems," Int. J. Control, Vol. 15, pp. 209-231, 1972.

26. Halyo, N. and R, E, Foulkes, "On the quadratic sampled-date regulator with unstable random disturbances," IEEE SMC soc. Proc. 1974 Internat. Conf. on Systems, Man and Cybern., pp. 99-103, October 2, 1974.

27. Bellman, R., Dynamic Programming, Princeton Univ. Press, Princeton, New Jersey, 1957.

28. Fortmann, T. E., "A non-recursive algebraic solution for the discrete Riccati equation," IEEE Trans. Auto. Control, pp. 597-599, Oct. 1970.

Appendix A

The aircraft equations of motion which are used in the simulation and for the development of the filter and control law were developed in Section II.A. The final form of the continuous equations as given in equation (50) is repeated here for convenience

$$\dot{x} = Ax + Bu + Dw$$

The form of the matrices A, B and D are also given in Section II.A. In this appendix, we shall give the expressions for the non-zero elements of these matrices in terms of the aircraft stability derivatives; the stability derivatives are assumed to be in the stability axis.

$$\alpha_1 = -\frac{mg\cos\theta_o}{\bar{q}_o S} \quad , \quad \alpha_2 = -\frac{mg\sin\theta_o}{\bar{q}_o S} \quad ,$$

$$\alpha_3 = \frac{mU_o}{\bar{q}_o S} \quad , \quad \alpha_4 = (\alpha_3 + C_{L\dot{\alpha}})^{-1} \quad ,$$

$$\alpha_5 = I_{yy}/\bar{q}_o S\bar{c} \quad , \quad \bar{q}_o = \frac{1}{2}\rho U_o^2 \quad ,$$

where S is the wing area, $\bar{c}$ the mean aerodynamic chord and ρ is the air density. Using these variables, the matrix elements are given below:

$$a_{14} = 1$$

$$a_{21} = \frac{\alpha_1}{\alpha_3} \quad , \quad a_{22} = \frac{1}{\alpha_3}\left(-C_{Du} - 2C_{Do} + C_{Txu} + 2C_{Txo}\right) ,$$

$$a_{23} = \frac{-C_{D\alpha} + C_{Lo}}{\alpha_3} \quad , \quad a_{27} = \frac{C_{Tx}}{\alpha_3} \quad , \quad a_{28} = -\frac{C_{D\delta s}}{\alpha_3} \quad ,$$

$$a_{31} = \alpha_2\alpha_4 \quad , \quad a_{32} = -\alpha_4(C_{Lu} + 2C_{Lo}), \quad a_{33} = -\alpha_4(C_{L\alpha} + C_{Do}) ,$$

$$a_{34} = \alpha_4(\alpha_3 - C_{Lq}) \quad , \quad a_{37} = \alpha_4 C_{Tz} \quad , \quad a_{39} = \alpha_4 C_{L\delta s} ,$$

$$a_{41} = \frac{\alpha_2\alpha_4}{\alpha_5} C_{m\dot{\alpha}} \quad , \quad a_{42} = \frac{1}{\alpha_5}\left(C_{mu} + 2C_{mo} + a_{32}C_{m\dot{\alpha}}\right),$$

$$a_{43} = \frac{1}{\alpha_5}\left(C_{m\alpha} + C_{mT\alpha} + a_{33}C_{m\dot{\alpha}}\right) \quad , \quad a_{44} = \frac{1}{\alpha_5}\left(C_{mq} + a_{34}C_{m\dot{\alpha}}\right) ,$$

$$a_{47} = \frac{C_{mT} + a_{37}C_{m\dot{\alpha}}}{\alpha_5} \quad , \quad a_{49} = \frac{C_{m\delta s} + a_{49}C_{m\dot{\alpha}}}{\alpha_5}$$

$$a_{77} = -.5 \quad , \quad a_{78} = .298 \quad ;$$

$$b_{21} = -\frac{C_{D\delta e}}{\alpha_3} \quad , \quad b_{31} = -\alpha_4 C_{L\delta e} \quad , \quad b_{41} = \frac{C_{m\delta e} + b_{31}C_{m\dot{\alpha}}}{\alpha_5}$$

$$d_{33} = \alpha_4(C_{L\dot{\alpha}} - C_{Lq}) \quad , \quad d_{43} = \frac{C_{mq} + (d_{33} - 1)C_{m\dot{\alpha}}}{\alpha_5}$$

Thus, given the stability derivatives of the aircraft, the A, B and D matrices can be computed.